AN ANALYSIS OF THE VARIABLE STAR, W VIRGINIS

Thesis by

Helmut Arthur Abt

In Partial Fulfillment of the Requirements
for the Degree of
Doctor of Philosophy

California Institute of Technology
Pasadena, California

1952

Acknowledgments

I wish to express my sincere gratitude to Dr. Jesse L. Greenstein for suggesting this investigation, starting me on the spectral observations, and providing many suggestions in the course of a number of discussions. I extend my thanks to Dr. Roscoe F. Sanford for the use of his Coude plates of W Virginis and of his radial velocities in advance of publication. And finally, I am grateful to Drs. Alfred E. Whitford and Arthur D. Code of Washburn observatory of the University of Wisconsin for obtaining the very important colors of W Virginis.

Abstract

W Virginis is a 17-day variable star which is considered to be the prototype of population II Cepheids. An analysis of the physical conditions in W Virginis during its cyclic variations has been made from the following data: High dispersion (10 Å/mm.) Coude plates were measured for radial velocities (by R.F.Sanford) and lines intensities which yielded curves of growth. Also used were a light curve in one color (Gordon and Kron) and colors (Whitford and Code).

The observations indicate an expansion of about 36×10^6 km. and then a subsequent contraction. The first indication of a new expansion wave is the appearance of hydrogen emission lines, formed deep in the atmosphere. Later the outward-moving region of gas produces absorption lines like that of an F-type star. These gain in strength until maximum expansion. This is also a time of minimum electron pressure and nearly minimum temperature. During the contraction the electron pressure, temperature, and opacity rapidly increase. Also just after maximum expansion the appearance of a new set of hydrogen emission lines from deep in the atmosphere indicates the start of a new outward-moving wave. There is a time of several days during which absorption lines are seen from the two masses of gas: the one falling downward and the other moving upward.

As the spectral features of the downward-moving region fade, those of the upward-moving region increase toward maximum strength. Data derived from the two simultaneous sets of absorption lines indicate very different conditions in the two regions.

It was found that relative radii derived from light and color curves could not be compared with displacements derived from the radial velocity curve, because, perhaps, the regions predominantly forming the continuous and line spectra have different motions. The extremely red colors and the large apparent temperature gradient, both particularly at maximum expansion, may be due to the presence of an extended atmosphere.

Table of Contents

I. Introduction

Cepheid variables are stars that show periodic changes in light and radial velocity. These changes have been fairly successfully attributed to radial pulsations. Eddington[1] has suggested that the large changes in the specific heats (by factors of 30 or 40), which accompany the ionization and recombination of hydrogen in the hydrogen convective zone of a star, may periodically dam up and release radiation to the other layers. He finds that the stars which should have well developed hydrogen convective zones are just the ones which fall in the region of the Cepheid variables in the mass-radius-luminosity diagrams.

Cepheid variables show a distinct concentration to the galactic plane, particularly in the regions of the supposed spiral arms, and are not present in globular clusters. They are clearly members of Baade's stellar population I [2]. However, there are variables in globular clusters that are somewhat related to the Cepheids. Although these stars have periods (1 to 50 days) like those of Cepheids, they have distinguishing characteristics. There are a few of these population II variables in the general field of stars in the galaxy, the brightest and best example being W Virginis. For this reason these population II variables, particularly those of periods 13 to 19 days, are called W Virginis variables.

W Virginis is identified as a population II variable rather than a classical Cepheid for the following reasons:

1) The light curve is abnormal for Cepheids: the maximum is much broader and has a shoulder on the decline.
2) The galactic latitude is large (+ 58°) so that the star is several thousand parsecs above the galactic plane.
3) The hydrogen lines appear in emission at some phases.
4) The radial velocity is high (about 65 km./sec.) and the proper motion is large for its distance (0.0103"), indicating that it is probably a high velocity star (its space velocity is 165 km./sec. for M= -2).
5) The changes in the star are not exactly periodic from cycle to cycle; this may possibly also be a distinguishing characteristic for population II variables.

It would be of value to make a study of W Virginis as an example of a population II counterpart of the classical Cepheids to obtain a model of the changes occurring in the star and a comparison with classical Cepheids.

II. Observations

A. Spectra

The spectra used were taken at the Coude focus of the 100-inch telescope on Mt. Wilson. The thirteen original plates taken by Dr. R.F. Sanford, principally near maximum light, were supplemented by nine similar plates taken near minimum light. Sanford measured all the plates for radial velocities and I used them to construct curves of growth from measured line intensities. Plates taken at similar phases by Sanford and myself gave similar results, indicating no systematic differences between the two sets.

In March 1949 the 114-inch collimating mirror and the 15,000 lines per inch Wood grating were replaced by a 184-inch collimator and a Babcock grating of 10,000 lines per inch. Since the Wood grating was used in the second order blue and the Babcock grating in the third order blue, all plates had about the same dispersion (10 Å/mm.). The Wood grating had the added feature that a piece of red sensitive plate could be put in the plateholder, along with the faster blue sensitive plate, to get the first order $H\alpha$ region. The Wood grating had some scattered light in the far ultraviolet region of the spectrum. The spectra are narrower with the new, long-focus collimator than with the previous collimator (0.16 and 0.26 mm.). Again no systematic differences were found between results from the two sets of plates taken with the different grating-collimator arrangements.

W Virginis (m_{pg} = 9.9 to 11.7) is the faintest star of which more than a few 100-inch Coude plates have been taken. Since there are known fluctuations in the physical parameters from cycle to cycle, every effort was made to obtain series of plates taken in single cycles. The following techniques were used to obtain the spectra:

1) An abnormally wide slit width was used for some of the plates. A normal slit width is one which gives the same projected image on the plate as the plate grain size, namely 12 to 20 μ. Slit widths up to 30 μ were used.
2) All plates were baked for three days at 50 °C just before exposure for added sensitivity. Eastman emulsions 103a-O and IIa-O were used.
3) The maximum exposure times allowed by the length of the night and the position of the star were generally used. These ranged from 3 to 8 hours but were still less than 2% of the period.

Step-slit calibration spectra, flanking the stellar spectra on the same plate, were given exposure times of not less than 10% of the stellar exposures.

Sanford's radial velocities are given in Table 1 and are plotted in Figure 1 against phases computed from eq.3. No phase corrections (see next section) were applied since all the computed corrections occur when the velocity curve is level. I am indebted to Dr. Sanford for permitting the use of his velocities prior to publication. The curve is discontinuous and shows that a new set (shortward components) of lines appears before the previous set (longward components) has vanished. These double lines are well resolved at this dispersion but were not detected by Joy[3] on his low dispersion plates. The velocities of the emission lines will be treated in section V.

An attempt was made to look for effects of stratification in the radial velocities. The lines of high excitation potential, E.P., should be formed predominantly at a lower level in the atmosphere than other lines. If different layers of the atmosphere have different outward velocities, there may be a variation of radial velocity with E.P. Four plates were measured completely and in some cases the Fe I lines (up to 200 per plate) of different E.P. showed radial velocity variations that were larger than the probable errors. However, these variations were not consistent between plates at similar phases in different cycles so that the results are inconclusive.

Table 1

Radial Velocity Measurements

Plate	Phase	Radial velocity in km./sec. Metals	H_{em}	H_{abs}
Ce 5058	0.283	-78.3		
5092	1.959	-40.3	-97.1	-39.9
5110	2.650	-49.2	-109.5	-65.4
5187	7.447	-71.6		-69.0
5216	9.242	-89.0		-93.5
5556	23.211	-91.2		-77.9
5616	25.981	-40.9	-105.4	-38.6
5617	26.042	-92.2 -42.2	-100.3	-40.1
5618	26.097	-91.6 -45.6	-94.0	-42.4
5647	28.005	-94.0 -43.1	-118.6	-38.7
5651	29.163	-94.9		-89.6
6207	46.945	-97.2 -42.6	- 85.5	-36.0
6211	47.004	-92.0 -37.0	- 84.2	-38.5
6889	66.814	-38.3	- 86.7	-36.0
6947	67.451	-73.9		
6965	68.604	-51.7		-53.4
7010	70.395	-67.1		
7013	70.452	-64.0		-56.0
7017	70.511	-59.5		-67.3
7080	72.709	-48.6	- 93.8	-53.6
7085	72.767	-44.2	- 94.1	-47.8
7091	72.825	-42.3	- 89.8	-42.3
7102	72.940	-92.8 -36.4	- 88.9	-40.2

Sanford has classified many of the spectra on the Mt. Wilson system and finds a variation from F2 at maximum light to G2 at minimum. From the almost complete absence of the G-band at minimum, the spectrum should not be later than GO, according to the Yerkes system[4]. The luminosity class is about Ib - certainly not II or III. The hydrogen lines, when in absorption only, are much too weak.

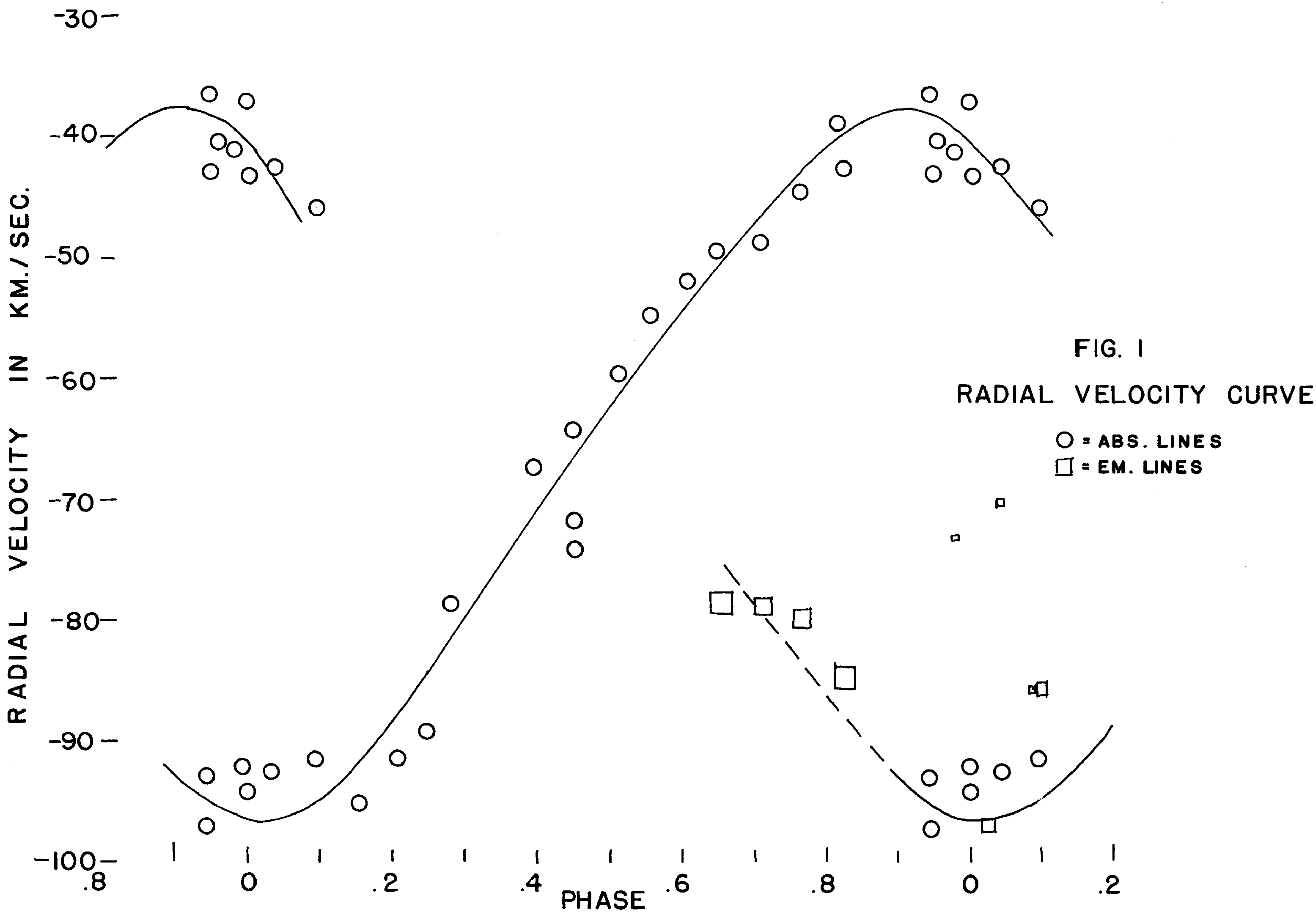

FIG. I

RADIAL VELOCITY CURVE

The hydrogen emission lines (Balmer series Hα to at least H8) vary a great deal from cycle to cycle but their general behavior is as follows: The lines are strong from minimum light (phase 0.65 ; see Fig. 4) to about phase 0.90, then fade and vanish at about phase 0.10 . There is always a much narrower absorption component present.

During some cycles (plates Ce 7102, Ce 6207 and 6211, but not Ce 5616-5618), when the emission and narrow absorption components are of about equal strength, a very broad, shallow absorption line is also present. This line has a central depth of less than 20% of the continuum and a half-width of 14 to 16 Angstroms. Fig. 2 shows Hδ on Ce 7102 on a density scale, showing the emission, absorption, and broad absorption components. Table 2 gives the smoothed intensity contour, $r = I_\lambda/I_c$, of the broad absorption line alone. Its center is within 10 km./sec. of the center of the emission line.

Table 2

Profile of the Broad Absorption Line, Hδ on Ce 7102

$\Delta\lambda = \lvert\lambda - 4100.5\rvert$	r	$\Delta\lambda$	r
1.5 A	0.809	6.5	0.895
2.5	.813	7.5	.928
3.5	.826	8.5	.969
4.5	.844	9.5	1.000
5.5	.862		

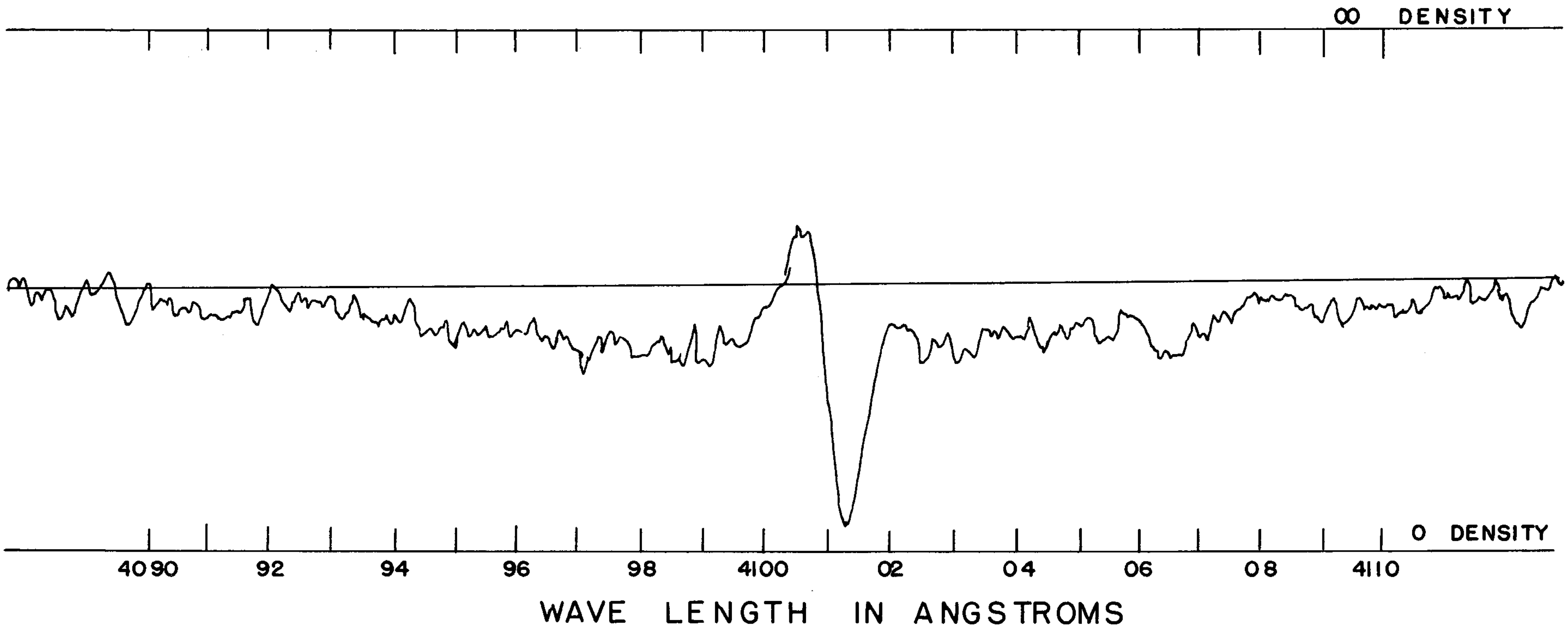

FIG. 2 Hδ ON PLATE CE 7102

B. Phases

Light observations have been made of W Vir since 1868. Using the best epochs of minimum as tabulated by A. Nielson[5], Sanford derived the following period:

$$\text{Phase of max. light} = 2432687.0 + 17.26944\ E, \qquad (1)$$

where E is the cycle number. Deviations of the observed from the calculated epochs of minimum are given in Table 3 and are plotted in Fig. 3. These seem to indicate the need for a second order term in the period but its nature is not yet clear. The epoch in Eq. 1 was chosen to fit the photoelectric observations of Gordon and Kron. A least squares solution, giving all epochs equal weight, gave

$$\text{Phase} = 2432688.41 + 17.27040\ E \qquad (2)$$

However, differences between Eqs. 1 and 2 are small and unimportant during the interval when the spectra were taken. The following equivalent of Eq. 1 will be used to calculate the preliminary phases in Table 4 :

$$\begin{aligned}\text{Phase of max. light} &= 2432687.0 - 7\times 17.26944 \\ &\qquad + 17.26944\ E \\ &= 2432566.114 + 17.26944\ E \qquad (3)\end{aligned}$$

All parameters measured for W Vir show differences from cycle to cycle which are larger than the expected probable errors. There may be two reasons for this: either 1) the system is not strictly periodic, or 2) the system is

Table 3

Epochs of Light Minimum

Obs. Epoch of Min.		O - C	Authority
JD 2404 150.94	(1871)	- 1.13 days	Schonfeld
2404 219.94	(1871)	- 1.21	Winnecke
2411 715.39	(1892)	- 0.69	Yendell
2414 841.37	(1899)	- .48	Wendell
2416 533.86	(1905)	- .40	Chant (A)
2419 246.23	(1913)	+ .67	Bemforad
2419 470.13	(1913)	+ .07	Chant (B)
2423 373.64	(1924)	+ .69	Haas
2424 997.53	(1928)	+ 1.24	Graff
2432 698.45	(1948)	.00	Gordon & Kron
2433 800.	(1951)	0.00 to +1.04	Whitford & Code
2424 300.	(1926)	+ 1.21	Joy (radial vel.)

periodic but the shape of the variations with phase is different, or more extreme, in one cycle than another. The actual situation may be a combination of the two cases.

Corrections to the preliminary phases could be made on the basis of several of the observed variable parameters, e.g. light, velocity, color, line strengths. It would not necessarily be true that each of these criteria would give the same corrections. However it was found, for instance,

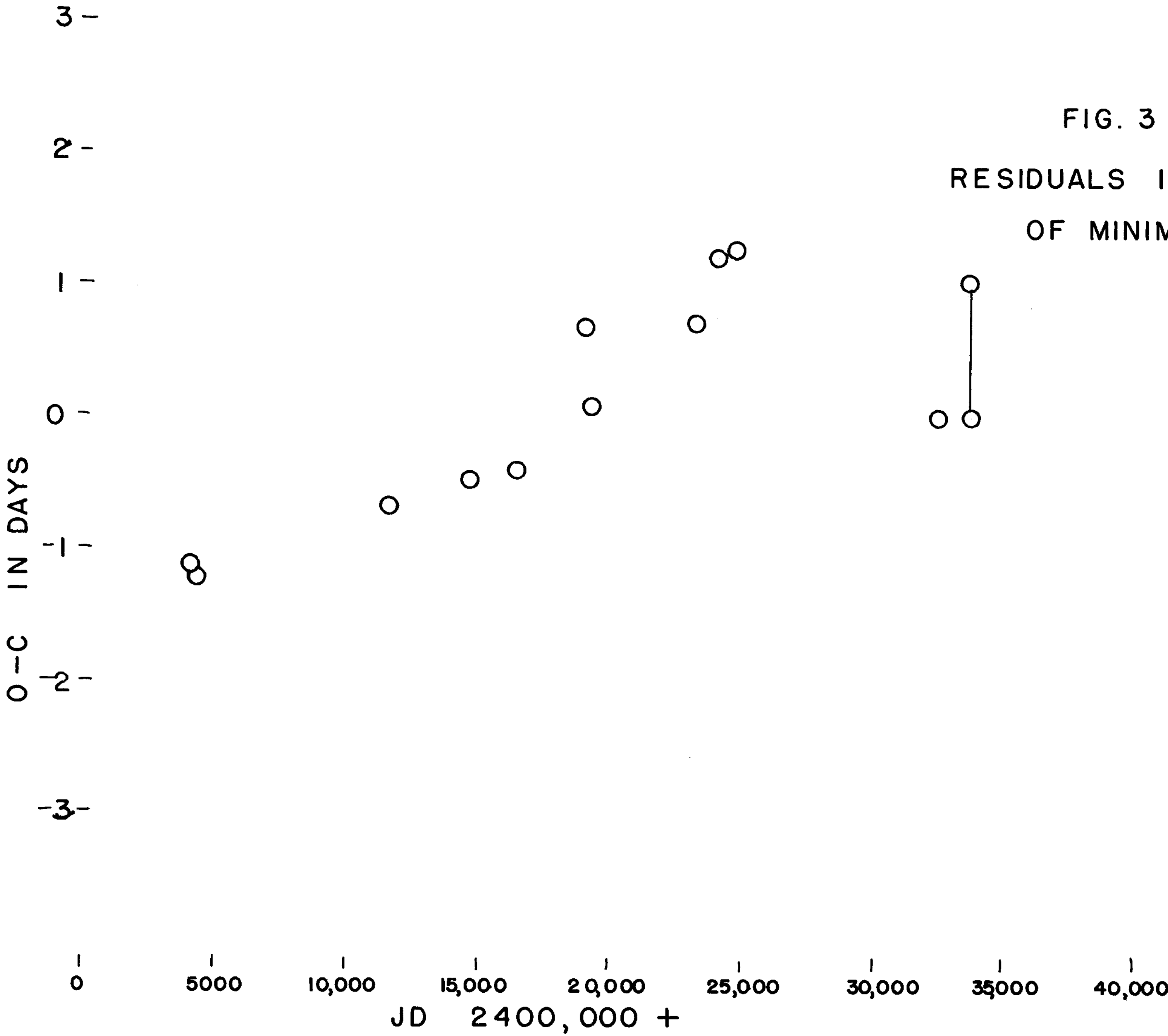

FIG. 3

RESIDUALS IN EPOCHS OF MINIMUM

Table 4

Preliminary Phases

Plate	Date & Time (PST) from Noon				JD	Cycle & Phase
Ce 5058	Jan.	19,	1948	14:30-18:00	2432 571.008	0.283
5092	Feb.	17,	"	12:25-17:00	599.946	1.959
5110	Feb.	29,	"	11:23-15:00	611.883	2.650
5187	May	22,	"	7:40-10:55	694.720	7.447
5216	June	22,	"	7:40-10:43	725.716	9.242
5556	Feb.	18,	1949	13:12-16:45	966.957	23.211
5616	April	7,	"	8:55-13:25	2433 014.799	25.981
5617	"	8,	"	9:30-15:00	015.843	26.042
5618	"	9,	"	8:25-13:25	016.788	26.097
5647	May	12,	"	8:15-11:55	049.753	28.005
5651	June	1,	"	7:50-12:00	069.746	29.163
6207	April	4,	1950	10:00-14:10	376.836	46.945
6211	"	5,	"	11:30-13:30	377.854	47.004
6889	March	13,	1951	12:38-17:08	719.954	66.814
6947	"	24,	"	13:03-16:48	730.955	67.451
6965	April	13,	"	9:20-16:10	750.864	68.604
7010	May	14,	1951	8:02-14:02	781.793	70.395
7013	"	15,	"	7:53-13:58	782.788	70.452
7017	"	16,	"	8:03-14:03	783.794	70.511
7080	June	23,	"	8:00-12:13	821.754	72.709
7085	"	24,	"	7:52-12:10	822.751	72.767
7091	"	25,	"	8:08-12:03	823.753	72.825
7102	"	27,	"	7:50-11:50	825.743	72.940

that the phase corrections derived from line strengths reduced the scatter in the temperature curves. In no case, however, did the phase corrections change the shape of a curve.

It was found that with the adopted preliminary phases, during the double line phase the change over from strong longward components to strong shortward components did not occur at the same phase each cycle. Since a knowledge of the physical parameters at the phases of double lines is particularly significant, it is desirable to make the data from various cycles consistent at these phases. The change in strength with time of the lines at these phases is very large. Hence I used the strength of two control lines, λ 4077 SrII and λ 4554 BaII, as a sensitive criterion of phase corrections. Table 5 gives the derived corrections. These data indicate that phase corrections (if necessary) for successive cycles are unrelated but during part of one cycle they are the same.

Table 5

Phase Corrections

Plate	Preliminary Phase	Corrected Phase	Correction
Ce 5058	.283	.358	+ .070
5556	.211	.196	- .015
5651	.163	.123	- .040
6207	.945	.040	+ .095
6211	.004	.089	+ .085
7102	.940	.030	+ .090

C. Light and Color Curves

At Sanford's request, Gordon and Kron [6] obtained a photoelectric light curve at about the same time as that of the first high dispersion spectroscopic observations. Their 1P21 photomultiplier tube and filter combination gave an effective wave length of 5000 A. An average of four observations on each of 16 nights were made during three cycles. At one maximum, Eggen [6] found the International photographic magnitude, P_{gp}, to be 10.13 . The zero point of their magnitudes at λ 5000 is otherwise unknown. Their observations are given in Fig. 4 .

At my request, Drs. A.E. Whitford and A.D. Code kindly consented to obtain colors of W Vir with the 60-inch telescope on Mt. Wilson in June and July, 1951. A refrigerated 1P21 photomultiplier tube was used behind a 1 mm. Schott BG12 filter or a 2 mm. Schott GG7 filter for blue and yellow magnitudes respectively. A Corning 7380 glass filter was used in all cases to cut out the far ultraviolet. The effective wave lengths, for stars with effective temperatures within a few thousand degrees of 5000°K, are 4260 and 5280 Å. No comparison star was used, but stars #11 and #52 in Selected Area 57 (at 33° from W Vir) were generally used as extinction stars. Single measures on 12 nights during two cycles were obtained. The weather was fair. International photographic magnitudes, P_{gp}, visual magnitudes, V, and photoelectric colors,

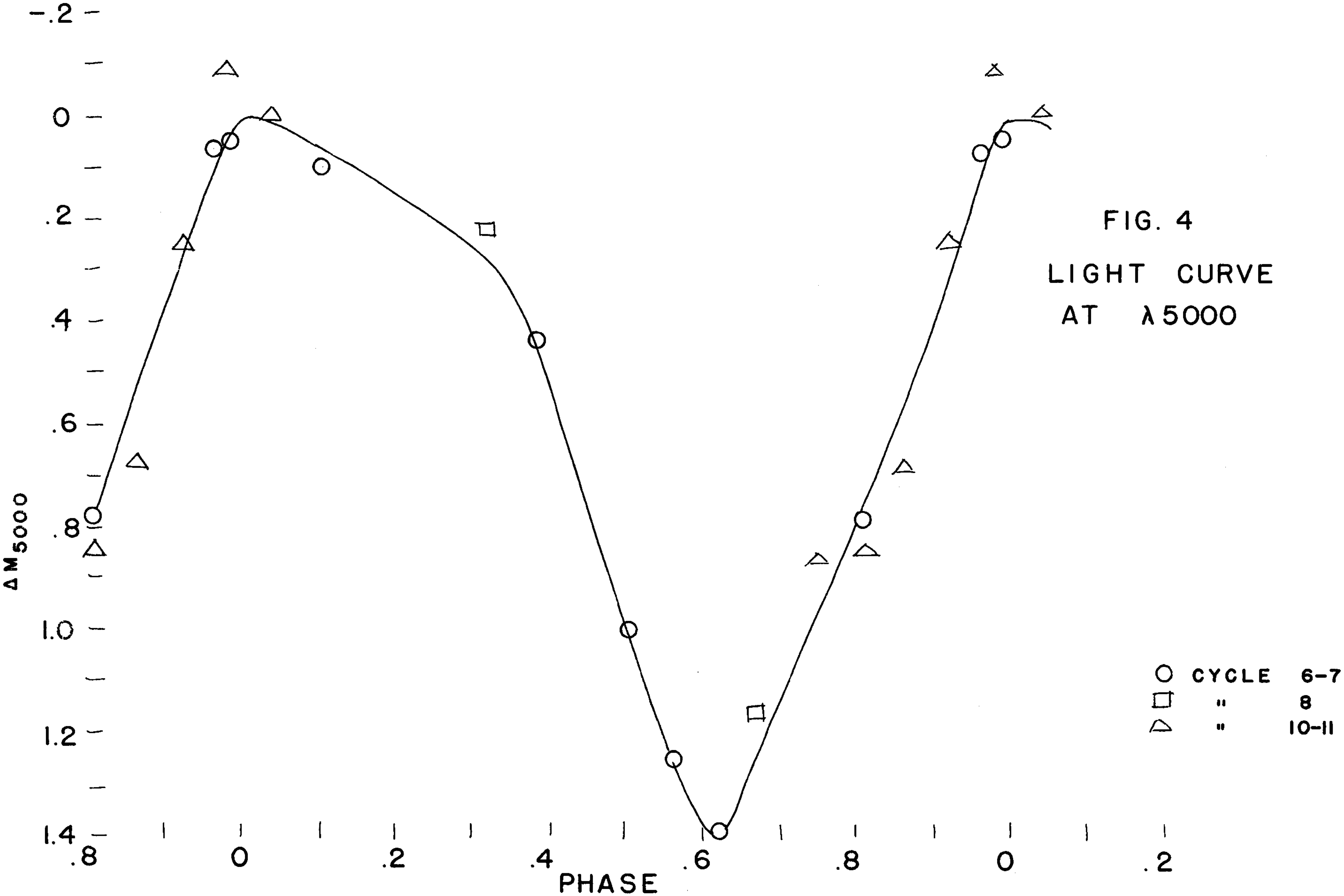

FIG. 4

LIGHT CURVE AT λ5000

C_p (which are the same as International colors, C_{int}), were obtained. Table 6 gives the data; the colors are plotted in Fig. 5.

There are probably not enough points to justify all parts of the color curve, i.e. the color at minimum light could be redder and the two points before maximum may be unusually blue. It is unfortunate that all the observations are from two cycles only since either or both of these cycles may have been unusual ones. However, we have no reason to suppose that the colors are not typical of most cycles. The probable error of their measurements is $\pm$ $0\overset{m}{.}02$, so the observed difference of $0\overset{m}{.}2$ between the two

Table 6

Colors and Magnitudes (Whitford and Code)

Date 1951	Time PST	JD	Cycle & Phase	C_p	P_{gp}	V
June 2	11:38	2433 800.804	71.496	+0.99	10.80	9.81
3	8:30	801.688	.547	.99	11.48	10.49
6	9:20	804.722	.723	.80	11.67	10.87
7	9:07	805.713	.780	.74	11.42	10.68
8	10:28	806.769	.841	.66	11.16	10.50
25	8:11	823.674	72.820	.48	10.75	10.27
26	8:05	824.670	.878	.29	10.34	10.05
30	8:21	828.681	73.110	.49	10.14	9.65
July 1	10:21	829.765	.173	.61	10.13	9.52
2	8:48	830.700	.227	.64	10.23	9.59
3	8:23	831.683	.284	.70	10.46	9.76
4	8.33	832.690	.342	.73	10.43	9.70

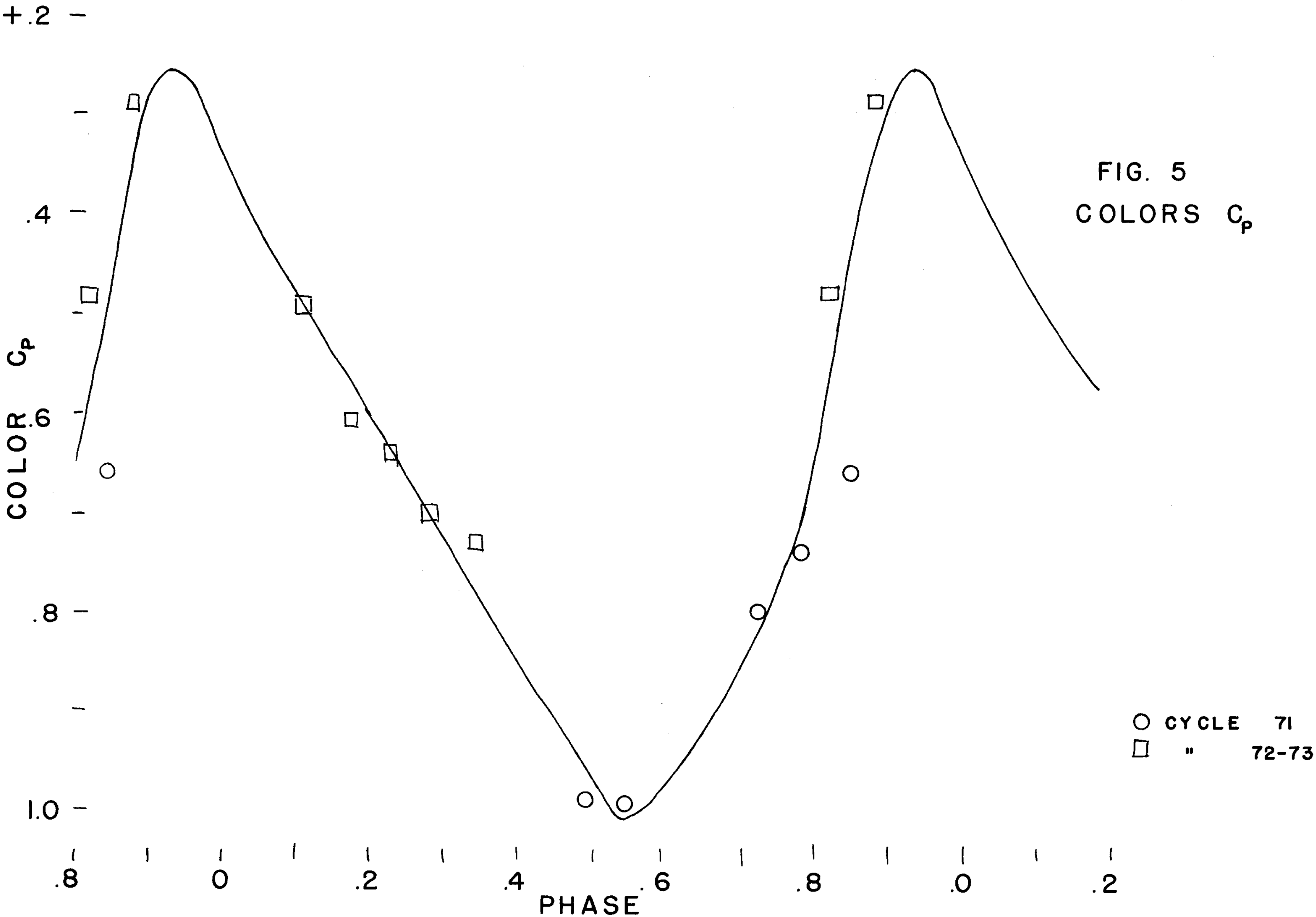

FIG. 5
COLORS C_P

cycles at phase 0.8 is intrinsic.

From Whitford and Code's observations at λ 4260 and λ 5280 and their colors we can obtain magnitudes at λ 5000, m_{5000}, from :

$$m_{5000} = m_{5280} + \frac{5280 - 5000}{5280 - 4260} C_p \qquad (4)$$

In Fig. 6 I fitted these observations as best I could to Gordon and Kron's light curve. We see that the observations in cycle 72-73 fit well enough, but those in cycle 71 are very discordant. Assuming a different epoch for Whitford and Code's observations would not help very much. This curve indicates P_{gp} = 9.88 at maximum, as compared with Eggen's value of 10.13 . Using 425 Harvard patrol plates, C.A.Chant[7] obtained a maximum photographic magnitude of 9.80, and S. Gaposhkin's survey of 713 Harvard plates yielded a maximum photographic magnitude of 9.85 . Since I cannot reconcile the Whitford-Code and Gordon-Kron measures, I will arbitrarily assume the following as representing the best data: 1) the light curve by Gordon and Kron for λ 5000, 2) colors by Whitford and Code, and 3) m_{4260} = 9.9 at maximum.

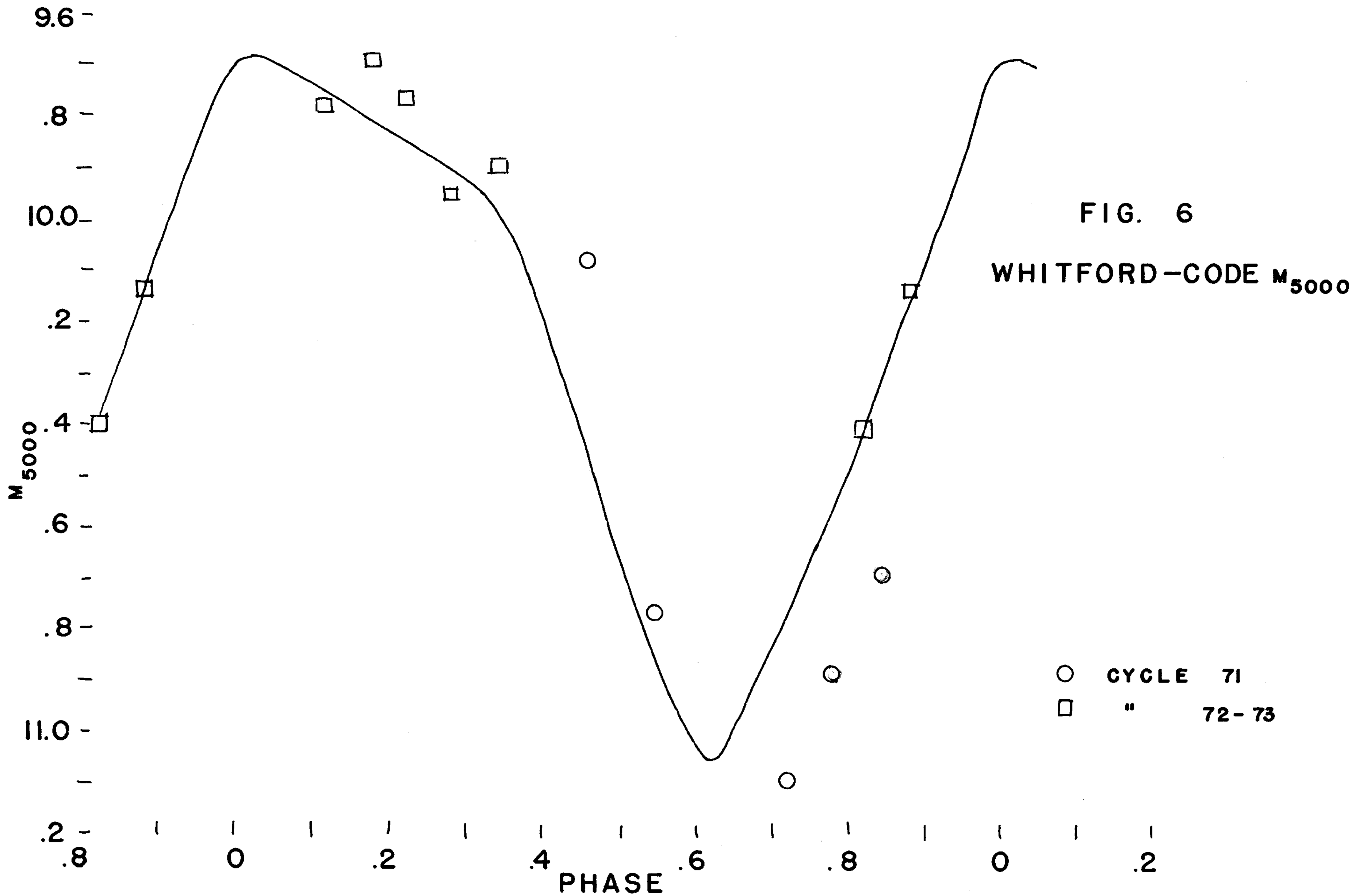

FIG. 6

WHITFORD-CODE M_{5000}

III. Spectraphotometric Reductions

A. Theory of Curves of Growth

In theoretical curves of growth we plot the logarithm of the absorption line strengths in units of the Doppler width against the logarithm of the ratio, η, of line to continuous absorption coefficients. The Doppler width, $\Delta\nu_D$, are

$$\Delta\nu_D = \overset{\nu}{\lambda} \frac{v}{c} = \frac{\overset{\nu}{\lambda}}{c} \left[\frac{2kT}{M} + v_T^2\right]^{\frac{1}{2}}, \tag{5}$$

where M is the mass of the atom in grams, T is the kinetic temperature, and v_T is the mean turbulent velocity. The line absorption coefficient per atom is

$$a_{\nu_0} = \frac{\sqrt{\pi}\, e^2}{mc} f \frac{1}{\Delta\nu_D} \tag{6}$$

Then if N_s is the number of atoms per gram in state s (i.e. capable of absorbing radiation at the wave length of the line), then at the center of the line,

$$\eta_0 = \frac{N_s\, a_{\nu_0}}{k_\nu}, \tag{7}$$

where k_ν is the continuous absorption coefficient. Then in terms of wave length units,

$$\eta_0 = \frac{\sqrt{\pi}\, e^2}{mc^2} \frac{Ngf\lambda}{vB(T_{ex})k_\lambda} 10^{-\theta_{ex}\chi}, \tag{8}$$

where N is the total number of atoms per gram, $B(T_{ex})$ is the partition function, $T_{ex} = \frac{5040}{\theta_{ex}}$ is the excitation temperature, and χ is the excitation potential. In the

Milne-Eddington model atmosphere we assume that the regions in which the lines and the continuous opacity are formed are coincident, or that η_0 is a constant with depth.

The shape of the curve of growth depends not only on the above parameters but also on the parameter a, which is proportional to the damping constant, Γ :

$$a = \frac{1}{4\pi} \frac{\Gamma}{\Delta\nu_D} \tag{9}$$

This includes both radiation and collisional broadening. The theoretical curves of growth used are those calculated for the total flux from a star on the Milne-Eddington model by Wrubel[8].

B. Measured Curves of Growth

1) Equivalent Widths

Microdensitometer tracings of the spectra were made at a magnification of 100. Using the step slit calibration spectra, intensity calibration curves were constructed every 200 Å. With these I converted densities on the tracings to relative intensities. For about 4/5 of the lines the calibration curves were sufficiently linear over the depth of the line that the line could be represented by a triangle and its equivalent width gotten from the central intensity and the base width in Angstroms. For the rest of the lines equivalent widths had to be gotten by a numerical integration method. When double lines were present the resolution was sufficient so that there was no difficulty with overlapping.

All the measured equivalent widths, W, in Angstroms are given in the Appendix.

2) Sources of Atomic Absorption Coefficients

The abscissae of the observational curves of growth are log $gf\lambda$. The f-values used for the FeI lines come from three sources: 1) the laboratory determinations by King and King[9] and Carter[10], 2) values derived from solar line intensities and curves of growth based on Kings' f-values by K.O. Wright[11], and 3) values derived from line strengths in the spectrum of τ Ursae Majoris by J.L. Greenstein[12]. Although the laboratory f-values are probably the most accurate, there are not enough of these available. Also they do not include the small, undetected blends that may be present in stellar spectra but not in laboratory spectra. The relative weights given to the above three sources are 3:1:1 in the order given. The zero points of the three log gfλ scales are different. A comparison of the log gfλ values for lines common to two or more sources give the following zero point corrections by least squares solutions:

$$\left[\log \eta_o(\tau) + 0.91\chi\right]_{JLG} - \left[\log gf\lambda\right]_{King} = -2.53 \pm .19 \qquad (10)$$

$$\left[\log \eta_o(\tau) + 0.91\chi\right]_{JLG} - \left[\log X_f + 1.04\chi\right]_{KOW} = 1.20 \pm .11 \qquad (11)$$

$$\left[\log \eta_o(\tau) + 0.91\chi\right]_{JLG} - \left[\log X_f + 1.04\chi\right]_{KOW} = 3.00 \pm .23 \qquad (12)$$

These equations were based on 33 FeI lines, 44 FeI lines, and 20 FeII lines respectively. Here $\log \eta_o(\tau)$ is the abscissa for τ Ursae Majoris for which $\theta_{ex} = 0.91$ and $\log X_f$ is the abscissa for the solar curves of growth for which $\theta_{ex} = 1.04$. No laboratory f-values for FeII are available. All scales of f-values were corrected to Greenstein's zero point before averaging. The final averaged values are given in the Appendix along with the equivalent widths.

3) Excitation Temperatures

The lines of FeI group themselves in groups according to excitation potential, E.P. (i.e. 0 to 0.12 ev.; .99 to 1.01 ev.; 1.48 to 1.60 ev.; etc.). Individual curves of growth were plotted for these EP groups; these should differ from each other only by the factor log $10^{-\theta_{ex}\chi}$ in the abscissae. Hence horizontal shifts, $\Delta \log \eta_0$, necessary to make them coincide will determine the excitation temperature, $T_{ex} = \frac{5040}{\theta_{ex}}$. A typical curve of horizontal shifts versus excitation potential for a plate is given in Fig. 7 . Actually the curves of growth for the EP groups were fitted individually to the adopted theoretical curve.

The excitation temperatures for FeII were assumed to be the same as for FeI.

4) Parameters of Curves of Growth

The parameters log a and log v/c were determined by fitting well defined curves of growth for sets of lines with nearly the same EP to the theoretical curves or by constructing composite curves from the various EP groups and fitting them to theoretical curves. A typical curve of growth is shown in

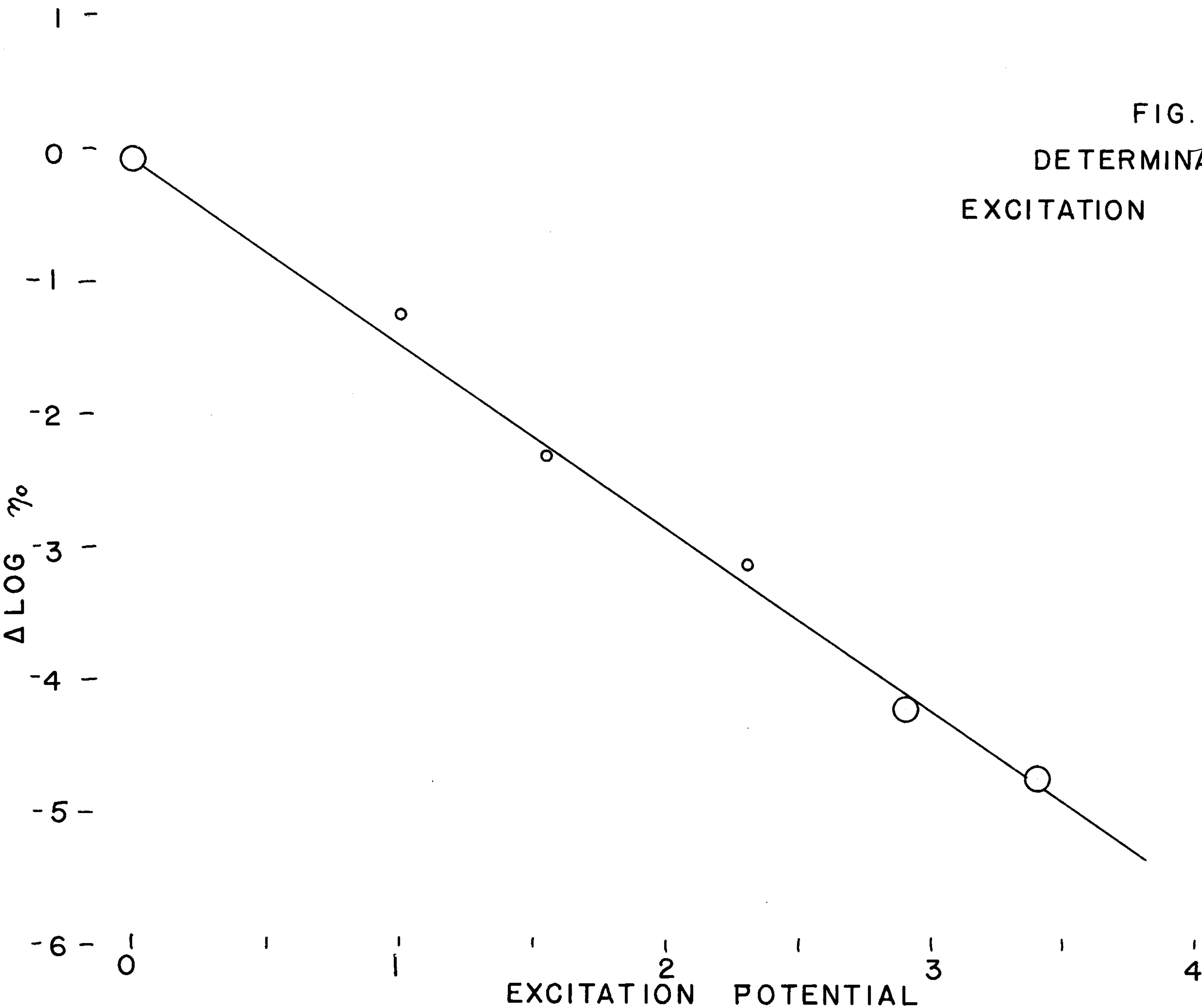

FIG. 7
DETERMINATION OF
EXCITATION TEMPERATURE

Fig. 8 .

The log f values that we have been using for FeI are correct on a relative scale, but the zero point is without meaning. We could put them on an absolute scale by subtracting[13] 3.73 from each log f on King's scale. However, these f-values would still be unrelated to those of FeII, so I chose to reduce the results by comparing my parameters with those from curves of growth for the sun, whose degree of ionization is known. After correcting for the EP of each line,

$$\log \frac{(\eta_o)_{W\,Vir}}{(\eta_o)_\odot} = \log \frac{(N/k)_W}{(M/k)_\odot} + \log \frac{(v/c)_\odot}{(v/c)_W} + \log \frac{B(T_{ex})_\odot}{B(T_{ex})_W} \qquad (13)$$

The parameters for the sun were found to be (using the same lines and f-values):

$$\begin{aligned} \log a &= -1.8 \\ \log v/c &= -5.13 \quad (\mathrm{FeI}) \\ &= -5.19 \quad (\mathrm{FeII}) \\ \log \eta_o &= .59 - 1.04 \quad (\mathrm{FeI}) \\ &= -3.84 - 1.04 \quad (\mathrm{FeII}) \end{aligned} \qquad (14)$$

The values of the partition functions, $B(T_{ex})$ were calculated has a function of excitation temperature only and values of log v/c for W Vir were obtained from the curves of growth. Hence we obtained values of $\log \frac{(N/k)_W}{(N/k)_\odot}$, the logarithm of

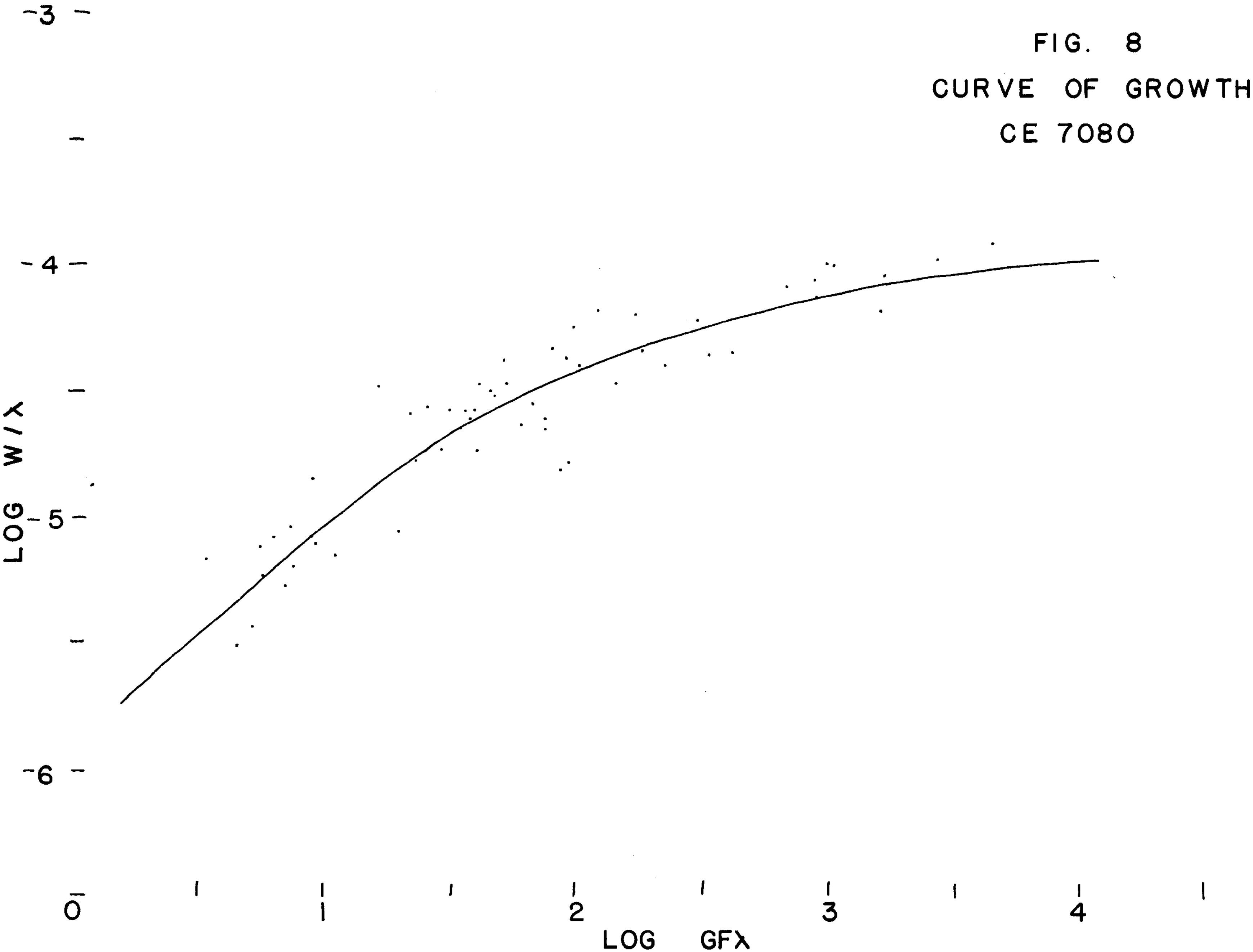

FIG. 8
CURVE OF GROWTH
CE 7080

the ratio of the FeI abundance to the continuous opacity for W Vir as compared to that in the sun. This ratio for FeII was found also, namely $\log \dfrac{(N'/k)_W}{(N'/k)_\odot}$. In Table 7 are listed in the order of corrected phase the parameters derived from the curves of growth. The quantities in parenthesis were assumed; these were all the excitation temperatures for FeII (assumed to be the same as for FeI), and some of the log a and log v/c (derived from plates at nearly the same phases). Seventeen plates, with an average of 105 lines per plate, were analyzed.

Table 7

Results from Curves of Growth

Plate	Phase Prelim	Phase Corr	Comp.	El.	log a	log v/c	θ_{ex}	$\log\frac{N/k}{N/k}$	# lines
Ce 5110	.650	.650		FeI	- 1.8	-4.76	1.46	0.39	90
				FeII	(- 1.8)	-4.70	(1.46)	1.48	17
7080	.709	.709		FeI	-1.8	-4.62	1.38	- .14	63
				FeII	(-1.8)	(-4.62)	(1.38)	.84	16
7085	.767	.767		FeI	-1.8	-4.49	1.28	- .99	75
				FeII	(-1.8)	(-4.49)	(1.28)	.24	17
7091	.825	.825	long.	FeI	(-1.8)	-4.45	1.12	-1.45	66
				FeII	(-1.8)	(-4.45)	(1.12)	- .25	18
			short.	FeI					11
				FeII					0
5616	.981	.981	long.	FeI	(-1.8)	-4.42	1.08	-2.48	35
				FeII	(-1.8)	(-4.42)	(1.08)	- .38	11
			short.	FeI					29
				FeII	(-1.8)	(-4.80)	(.96)	-1.31	11
								± .28	

Ce	5647	.005	.005	long.	FeI	(-1.8)	-4.49	1.11	-1.82	37
					FeII					0
				short.	FeI					24
					FeII					0
	7102	.940	.030	long.	FeI	(-1.8)	-4.35	1.13	-2.97	16
					FeII	(-1.8)	-4.60	(1.13)	- .42	9
				short.	FeI	-1.8	-4.76	.96	-1.78	70
					FeII	-1.8	-4.90	(.96)	- .01	18
	6207	.945	.040	long.	FeI					10
					FeII	(-1.8)	(-4.50)	(1.25)	- .59	7
									± .27	
				short.	FeI	(-1.8)	-4.66	1.09	-1.62	77
					FeII	(-1.8)	-4.80	(1.09)	.28	17
	5617	.042	.042	long.	FeI	(-1.8)	-4.40	1.10	-2.33	53
					FeII	(-1.8)	(-4.40)	(1.10)	- .98	4
				short.	FeI	(-1.8)	-4.80	.94	-2.12	75
					FeII	(-1.8)	(-4.80)	(.94)	-1.28	7
	6211	.004	.089	long.	FeI					6
					FeII					0
				short.	FeI	(-1.8)	-4.64	1.05	-1.33	97
					FeII	(-1.8)	-4.58	(1.05)	.04	19
	5618	.097	.097	long.	FeI	(-2.2)	-4.40	1.36	-2.27	26
					FeII	(-2.2)	(-4.40)	(1.36)	- .77	5
				short.	FeI	-2.2	-4.78	1.07	-1.38	69
					FeII	(-2.2)	-4.86	(1.07)	.45	16
	5651	.163	.123		FeI	-2.2	-4.80	1.25	- .42	131
					FeII	-1.8	-4.80	(1.25)	.79	19
	5556	.211	.196		FeI	-2.2	-4.74	1.22	- .11	80
					FeII	-1.8	-4.86	(1.22)	1.36	15
	5058	.283	.358		FeI	-2.2	-4.68	1.18	- .17	72
					FeII	-2.2	-4.86	(1.18)	1.79	18
	7010	.395	.395		FeI	-1.8	-4.78	1.29	- .07	112
					FeII	-2.2	-4.84	(1.29)	1.62	20
	7013	.452	.452		FeI	-1.8	-4.70	1.28	- .01	125
					FeII	-2.2	-4.80	(1.28)	1.53	21
	7017	.511	.511		FeI	-2.2	-4.63	1.27	.07	112
					FeII	-1.8	-4.74	(1.27)	1.26	19

C. Discussion and Calculations of Parameters from Curves of Growth

1) Damping Constants

The values of the damping constant parameters, log a, were found to be normal, namely -1.8 and -2.2 . The differences in log a for neutral and ionized elements is probably not real. It is not certain whether there is a real variation of log a with phase.

Because of the large Doppler velocities, the actual damping constant, Γ , came out rather large (see eq. 9). For normal supergiants and dwarfs, the value of Γ/γ_{cl} varies from about 2 to 10 (ref. 11,12,14). For W Vir this ratio varied from 7 to 35. The probable error in log a is $\pm$ 0.4 and therefore in Γ/γ_{cl} the probable error is a factor of $2\frac{1}{2}$.

2) Doppler Velocities

Doppler velocities, log v, are plotted in Fig. 9 . For kinetic temperatures of 7200° and 4600° the thermal velocity varies from only 1.46 to 1.17 km./sec. Since the Doppler velocity dispersion varies from 4.7 to 12 km./sec., the changes must be due mostly to changes in turbulent velocity. The term "turbulent velocity" is used loosely here: the atmosphere may have turbulent motion with a normal turbulent spectrum, or the motion may be like that of solar prominences or in streams, i.e. large mass motion of streamers

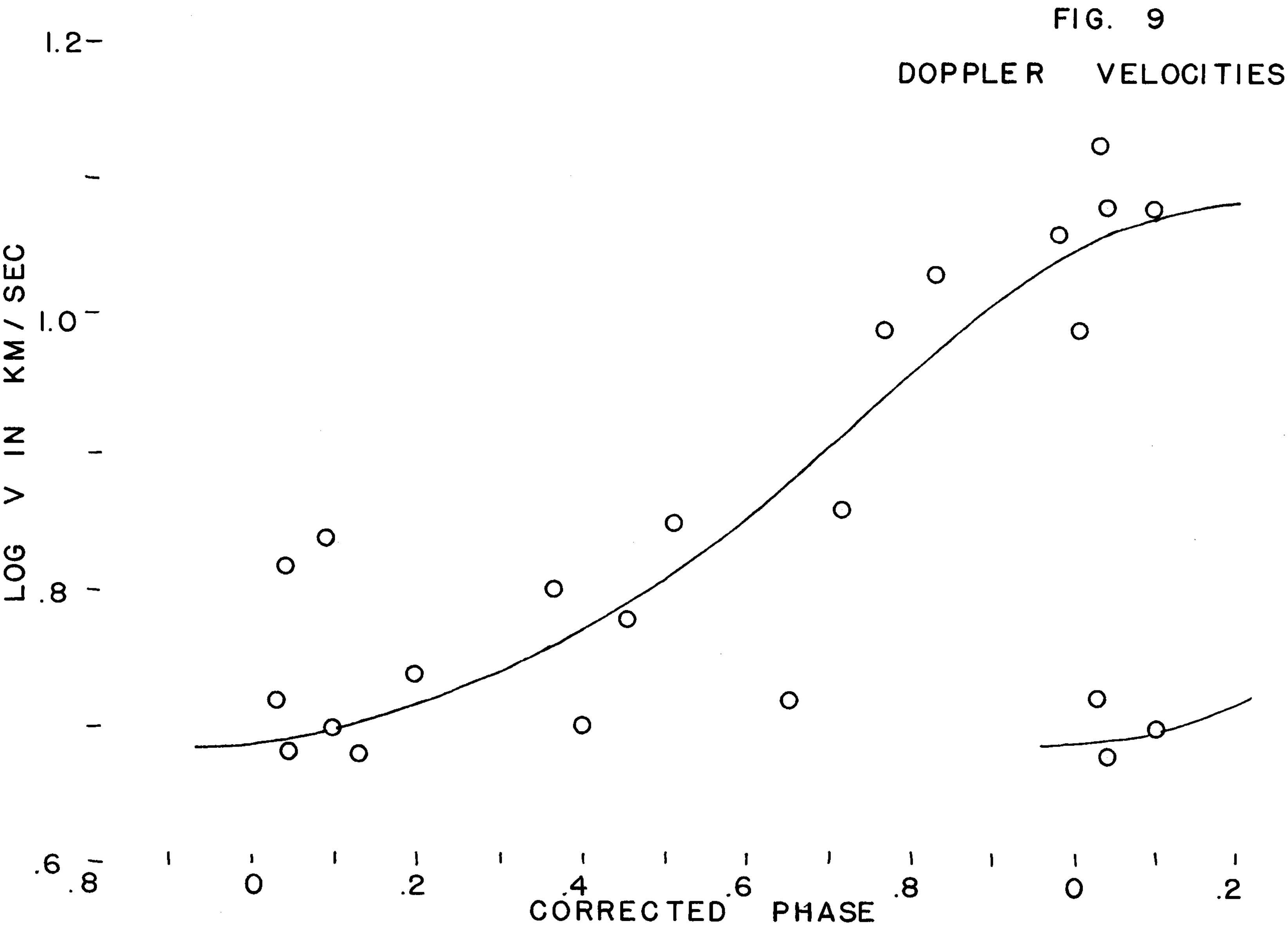

FIG. 9

DOPPLER VELOCITIES

of gas, causing multiple but unresolved line components. The instrumental profile corresponds to 10 to 20 km./sec., so that such components could not be detected.

Fig. 9 shows that the turbulent velocity increases with phase. Furthermore, three plates with double lines yielded simultaneous determinations of the Doppler velocity for both components. Without question, the shortward (or new) components have the smaller turbulent velocities.

Errors of photometry apply directly to the resulting values of log v/c. However, no systematic differences were found between Sanford's (older) plates and my (newer) ones.

3) Excitation Temperatures

Excitation temperatures for FeI are plotted in Fig. 10 . The curve is well defined and shows the following: The new, shortward components (phase 0) show a rapid decrease from a high temperature. The minimum temperature is reached at minimum light (phase 0.65). Three plates with double lines yielded individual excitation temperatures for each set of lines; the shortward components of these are plotted a second time, at the right side of the diagram. The difference in excitation temperature for the two sets of lines is 800° to 1000°, with the shortward component giving the higher temperature. The longward component seems to show a rapid drop

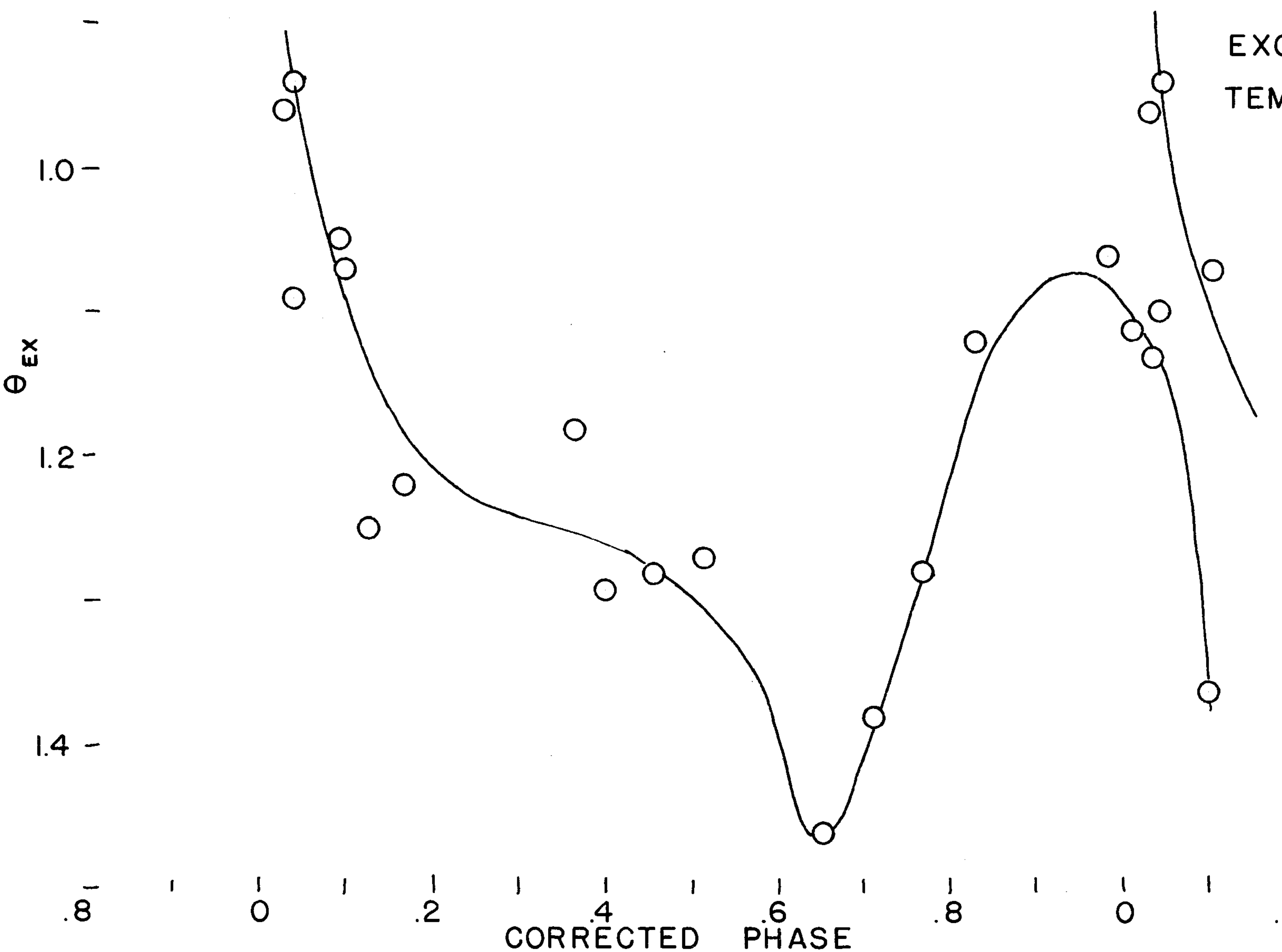

FIG. 10
EXCITATION
TEMPERATURES

in temperature just before it disappears (phase 0.1). This seems to be especially valid since two of these three plates were taken on successive nights and the second shows a marked drop in temperature for both sets of lines. All the excitation temperatures derived are very low for an F or early G-type star.

4) Ratio of Abundance to Opacity

The ratio of abundance of FeI and FeII to continuous opacity for W Vir compared to that in the sun ($\log \frac{N/k}{(N/k)_\odot}$ and $\log \frac{N'/k}{(N'/k)_\odot}$) are plotted in Figs. 11 and 12. Since it is not likely that the total amount of iron per gram of stellar material varies with phase, the variations shown in Figs. 11 and 12 must be due to changes in degree of ionization and in opacity.

5) Ionization temperatures and Electron Pressures

We shall now calculate the ionization temperatures and electron pressures from the quantities just derived. In Table 8 we give the ordinates of the smoothed curves drawn in Figs. 11 and 12. The ratio of the two quantities is the relative degree of ionization, $\log \frac{N'/N}{(N'/N)_\odot}$, and is independent of opacity. This ratio has also been slighty smoothed out. We can calculate the degree of ionization in the sun from the known mean parameters for the solar atmosphere [15], namely

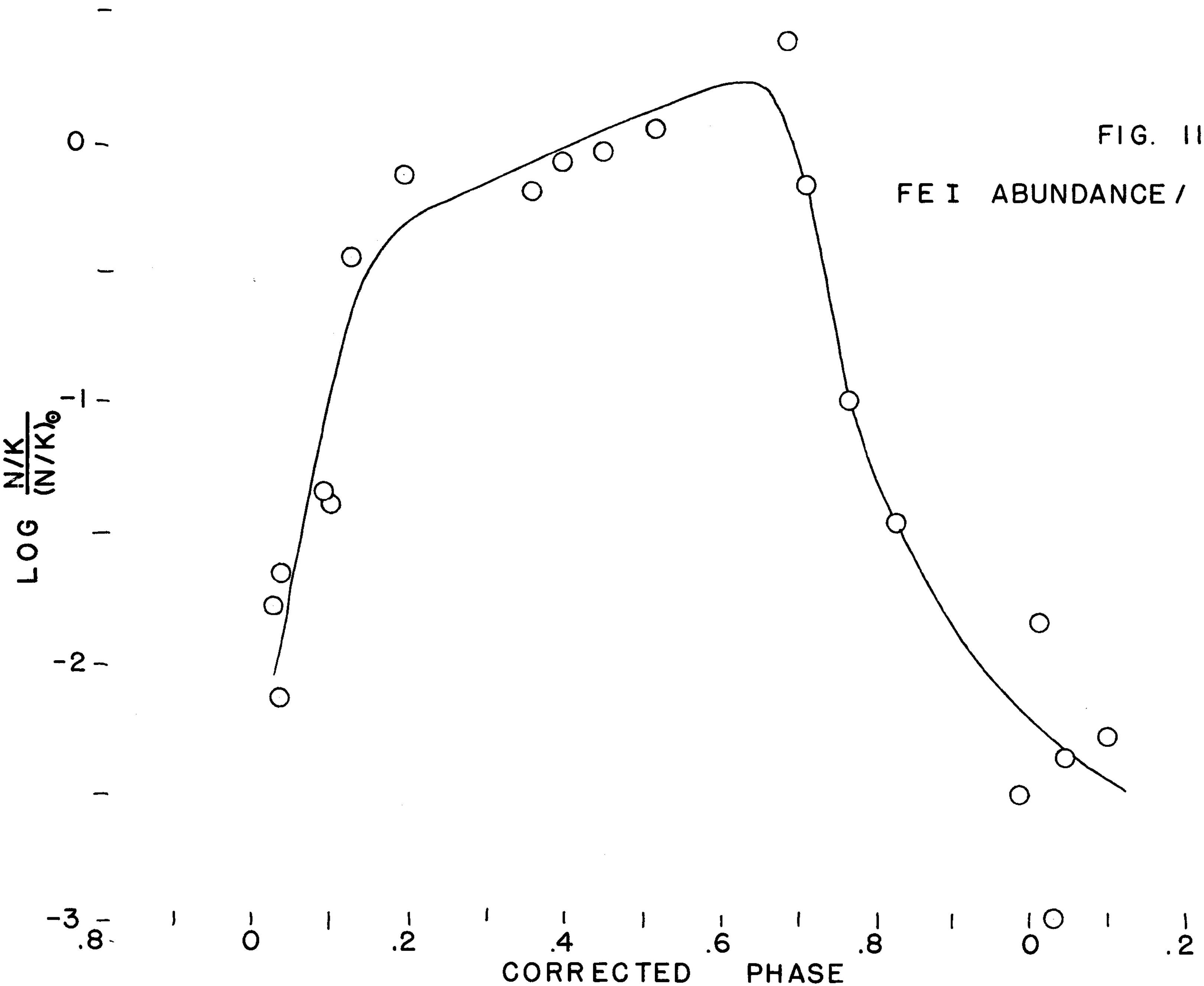

FIG. 11

FE I ABUNDANCE / OPACITY

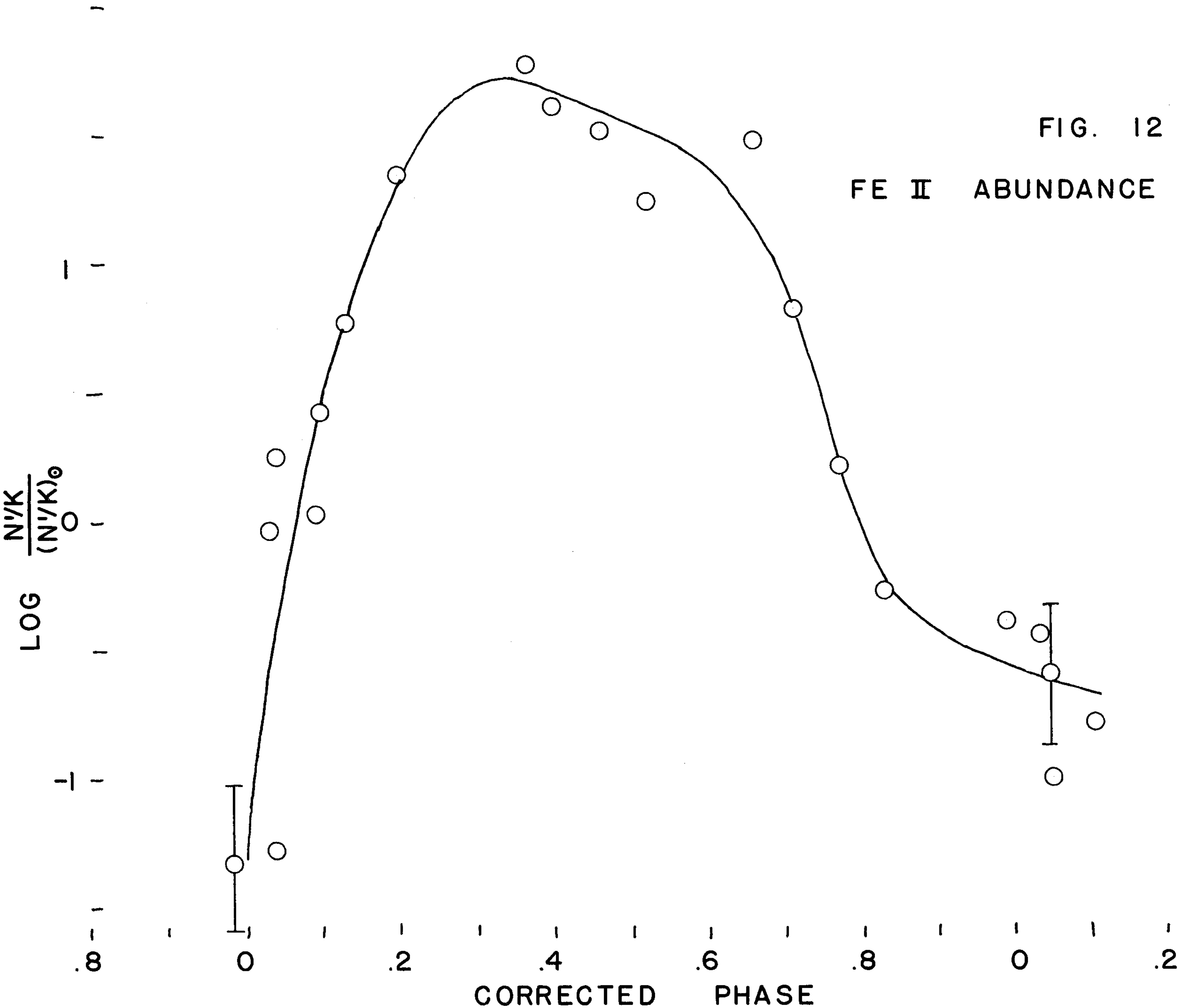

FIG. 12

FE II ABUNDANCE / OPACITY

Table 8

Ionization and Electron Pressures

Phase	Smoothed $\log\frac{N/\bar{k}}{(N/\bar{k})_\odot}$	$\log\frac{N'/\bar{k}}{(N'/\bar{k})_\odot}$	$\log N'/N$	$A = A_\odot$: $\log\bar{k}$	θ_{ion}	$\log P_e$	$A = 3A_\odot$: $\log\bar{k}$	θ_{ion}	$\log P_e$
.00		-1.30							
.05	-1.74	-.13	2.35	-.03	.73	1.51	-.51	.78	.99
.10	-.89	.50	2.43	-.94	.83	.55	-1.42	.89	-.05
.15	-.43	1.00	2.55	-1.50	.89	-.13	-1.98	.945	-.64
.20	-.29	1.35	2.70	-1.79	.91	-.45	-2.27	.97	-1.00
.25	-.21	1.57	2.85	-2.01	.92	-.71	-2.49	.99	-1.32
.30	-.14	1.71	2.91	-2.14	.93	-.85	-2.62	.99	-1.41
.35	-.08	1.72	2.86	-2.15	.93	-.83	-2.63	1.00	-1.42
.40	.00	1.68	2.74	-2.11	.94	-.78	-2.59	1.01	-1.40
.45	.07	1.61	2.61	-2.05	.95	-.74	-2.53	1.02	-1.35
.50	.13	1.54	2.47	-1.96	.95	-.61	-2.44	1.025	-1.28
.55	.19	1.46	2.34	-1.89	.96	-.56	-2.37	1.03	-1.20
.60	.23	1.36	2.20	-1.78	.965	-.47	-2.26	1.04	-1.11
.65	.20	1.20	2.07	-1.61	.96	-.29	-2.09	1.03	-.89
.70	-.09	.90	2.07	-1.33	.92	.08	-1.81	.99	-.55
.75	-.80	.39	2.17	-.73	.825	.82	-1.21	.895	.18
.80	-1.30	-.06	2.28	-.36	.775	1.19	-.84	.83	.69
.85	-1.60	-.30	2.40	-.19	.75	1.30	-.67	.80	.83
.90	-1.83	-.41	2.52	-.09	.72	1.41	-.57	.78	.88
.95	-2.03	-.48	2.63	.00	.71	1.43	-.48	.765	.92
1.00	-2.19	-.54	2.73	.06	.695	1.46	-.42	.755	.92
1.05	-2.32	-.60	2.79	.14	.69	1.47	-.34	.745	.95
1.10	-2.43	-.64	2.86	.21	.665	1.60	-.27	.73	.99

$(\theta_{ion})_\odot = 0.95$, $(\theta_{ex})_\odot = 1.04$, and $\log (P_e)_\odot = 0.80$. Saha's ionization can be written as:

$$\log \frac{N'}{N} = -I\,\theta_{ion} - \frac{5}{2}\log \theta_{ion} + 9.08 + \log \frac{B'(T_{ex})}{B(T_{ex})} - \log P_e \qquad (15)$$

For iron in the sun, $\log N'/N = 1.07$. Also $\log N''/N' = -6.8$, so there is no appreciable amount of FeIII in the solar atmosphere. The logarithm of the degree of ionization, log N'/N, for W Vir is then given in Table 8 and is plotted in Fig. 13 . We see that the degree of ionization is high but does not vary much, considering the large changes in temperature. We can expect large density changes.

Having the degree of ionization, we have a relation (eq. 15) between θ_{ion} and P_e. We need another such relation to obtain both these quantities. Such a relation is the equation for the continuous opacity, which is a function of θ_{ion}, P_e, and the hydrogen to metal ratio, A.

The continuous opacity in F stars is due mainly to H^- and partly to H, and is given by

$$\bar{k} = \frac{1-x_H}{m_H}\left[a(H^-)\ P_e + a(H)\right], \tag{16}$$

where $\bar{k}$ = mean (over wave length) opacity per gram

x_H = degree of ionization of hydrogen = $\frac{N(HII)}{N(HI) + N(HII)}$

$a(H^-)$ = absorption coefficient per H^- ion

$a(H)$ = " " " H atom.

The $a(H^-)$ and $a(H)$ are functions of temperature only and are given by Chandrasekhar and Münch[16]. Also x_H can be calculated from the ionization equation for H as a function of θ_{ion} and P_e. Hence $\bar{k}$ can be known as a function of $_{ion}$ and P_e.

We can obtain observational values of the mean opacity $\bar{k}$ from the quantity $\log \frac{N/k}{(N/k)_\odot}$ if we make four assumptions. First, since the source of opacity is probably mostly due to H^- in W Vir as it is in the sun, the ratio

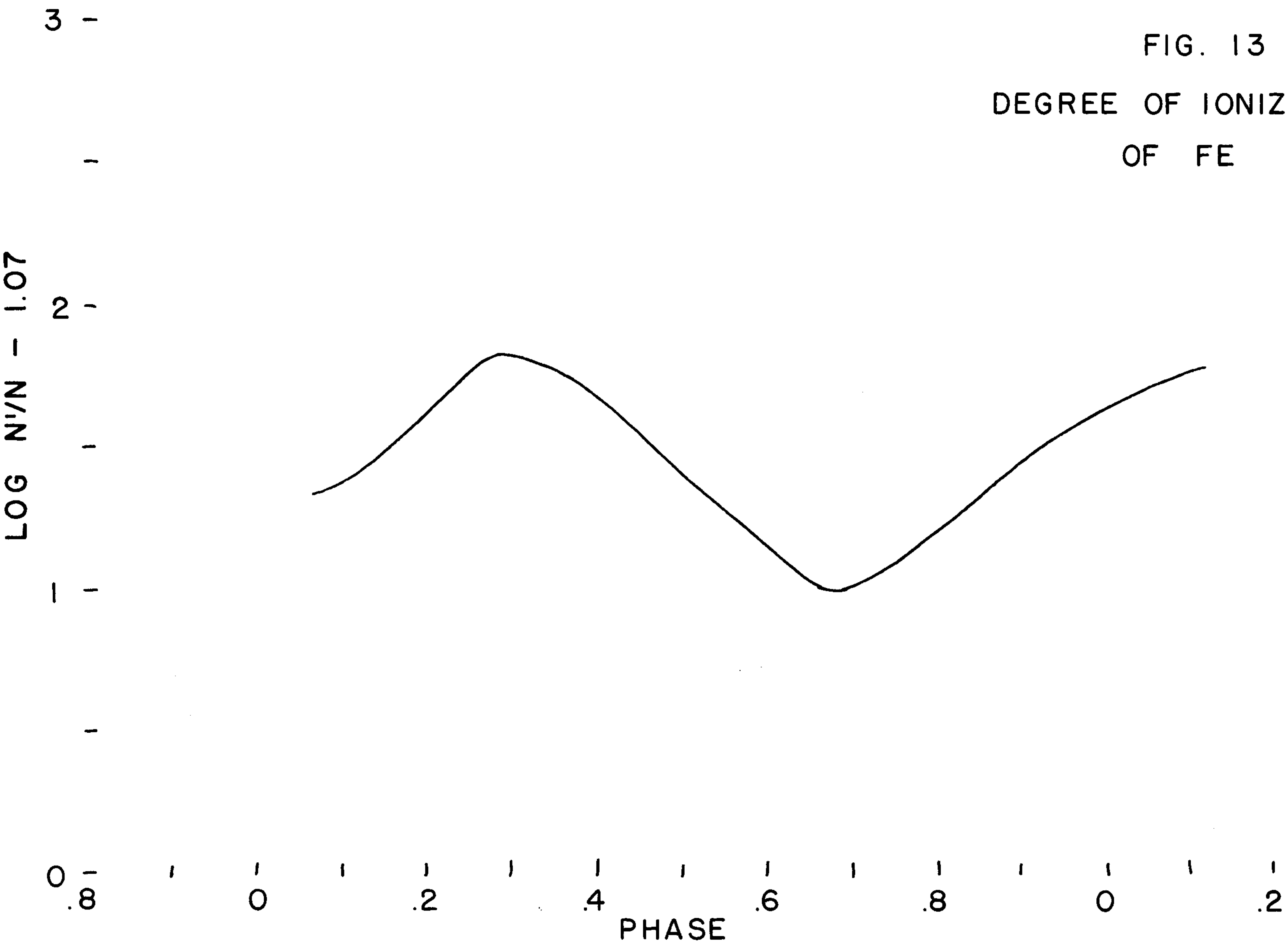

FIG. 13

DEGREE OF IONIZATION OF FE

between the opacity in the photographic region and the mean opacity should be the same, i.e.

$$(k/\bar{k})_W = (k/\bar{k})_\odot \qquad (17)$$

Next we must make an assumption about the hydrogen to metal ratio in W Vir. There is some indication[17] that high velocity stars may have a smaller metal abundamce, or a larger A, by a factor 3 then low velocity stars. Unfortunately we will not be able to get an explicit determination of A and our ionization temperatures and electron pressures will depend on the value of A chosen. We will calculate θ_{ion} and P_e for both the solar abundance, $A = A_\odot$, and the suggested high velocity star abundance, $A = 3A_\odot$.

Our third assumption concerns the amount of FeIII present. We will assume, for the time being, that its abundance depends entirely on the local ionization temperature and electron pressure in the atmosphere. This is a normal assumption in a normal star, but in W Vir it may be that there is an additional source of ionizing radiation just after minimum light in Lyman emission lines and Lyman continuum. Neglecting this possibility for the present, we calculate that the amount of FeIII present is neglible. In fact, almost all iron will be singly ionized (FeII).

As a fourth assumption, we will neglect the effects of the composite spectrum during the phases of double lines (phases 0.8 to 0.1). The strength of the lines formed at lower levels is reduced the overlapping continuous emission; that of the lines formed at higher levels is less affected. For the time being, we must realize that the determination of $\bar{k}$ is subject to considerable corrections for phases 0.8 to 0.1 .

With these four assumptions it becomes possible to determine $\bar{k}$, knowing that $\log (\bar{k})_{\odot} = -0.535$, and hence to relate θ_{ion} and P_e by equation 16. Then for each phase I plotted the relation between θ_{ion} and P_e which gives the observed opacity and the relation which gives the observed degree of ionization. A sample curve is given in Fig. 14. The intersection of the two curves gives the desired values of θ_{ion} and P_e. The resulting values of $\log \bar{k}$, θ_{ion}, and $\log P_e$ are tabulated in Table 8 and are plotted in Figs. 15, 16, and 17 for both values of A. The resulting ionization temperatures show a minimum at minimum light (phase 0.65) but the amplitude is much smaller than for the excitation temperatures. The ionization temperatures are much higher and the difference between the temperatures of the longward and shortward components is reduced..

To check on the θ_{ion} and $\log P_e$ derived for FeI, the same were obtained at one phase for the Ca lines, K and λ 4226, for which absolute f-values are known.[18] On plate Ce 7010 at phase 0.395 we obtained for Ca: $\theta_{ion} = 1.04$ and $\log P_e = -0.35$, while for Fe we obtain $\theta_{ion} = .94$ and

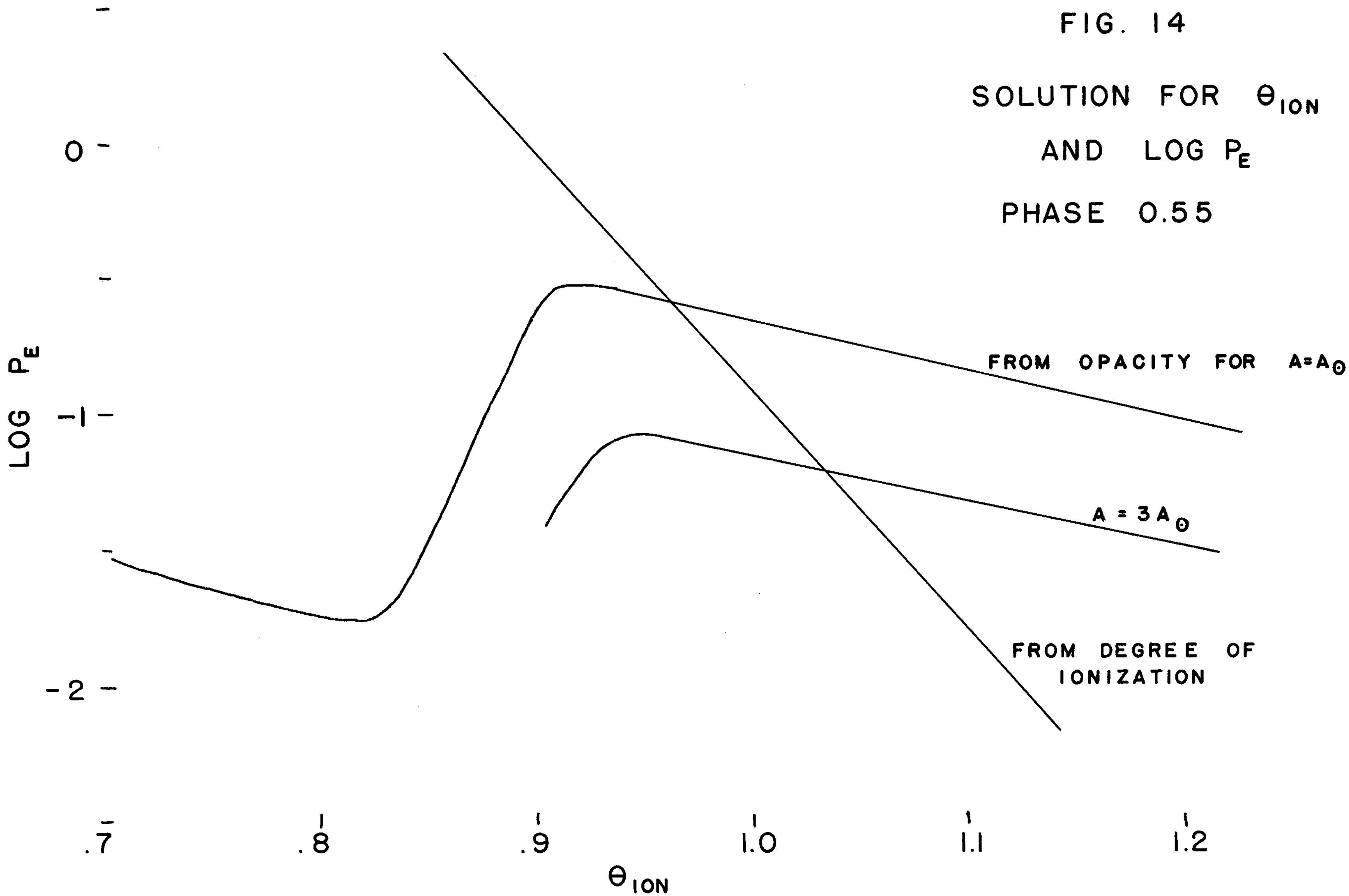

FIG. 14

SOLUTION FOR θ_{ION} AND LOG P_E

PHASE 0.55

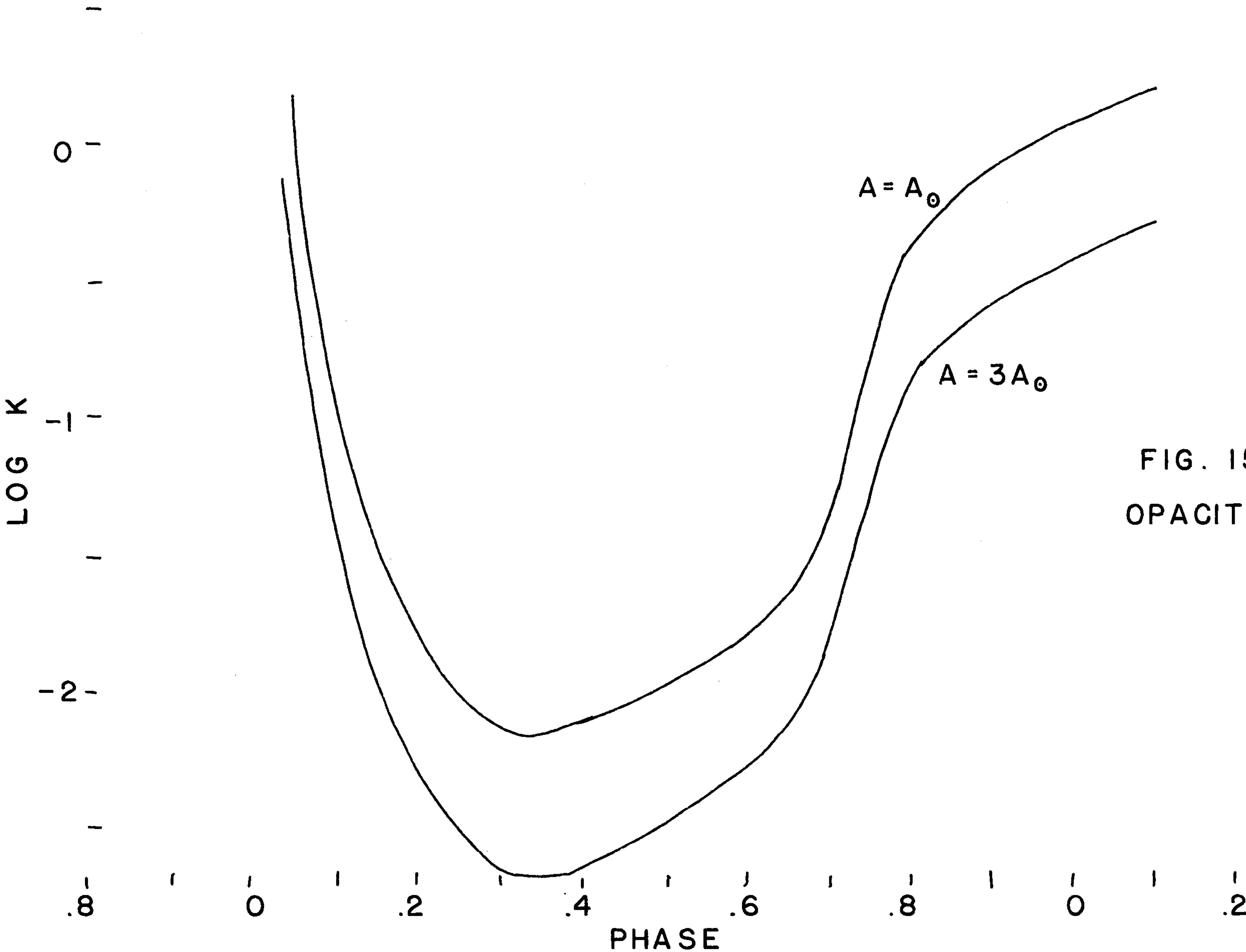

FIG. 15
OPACITY

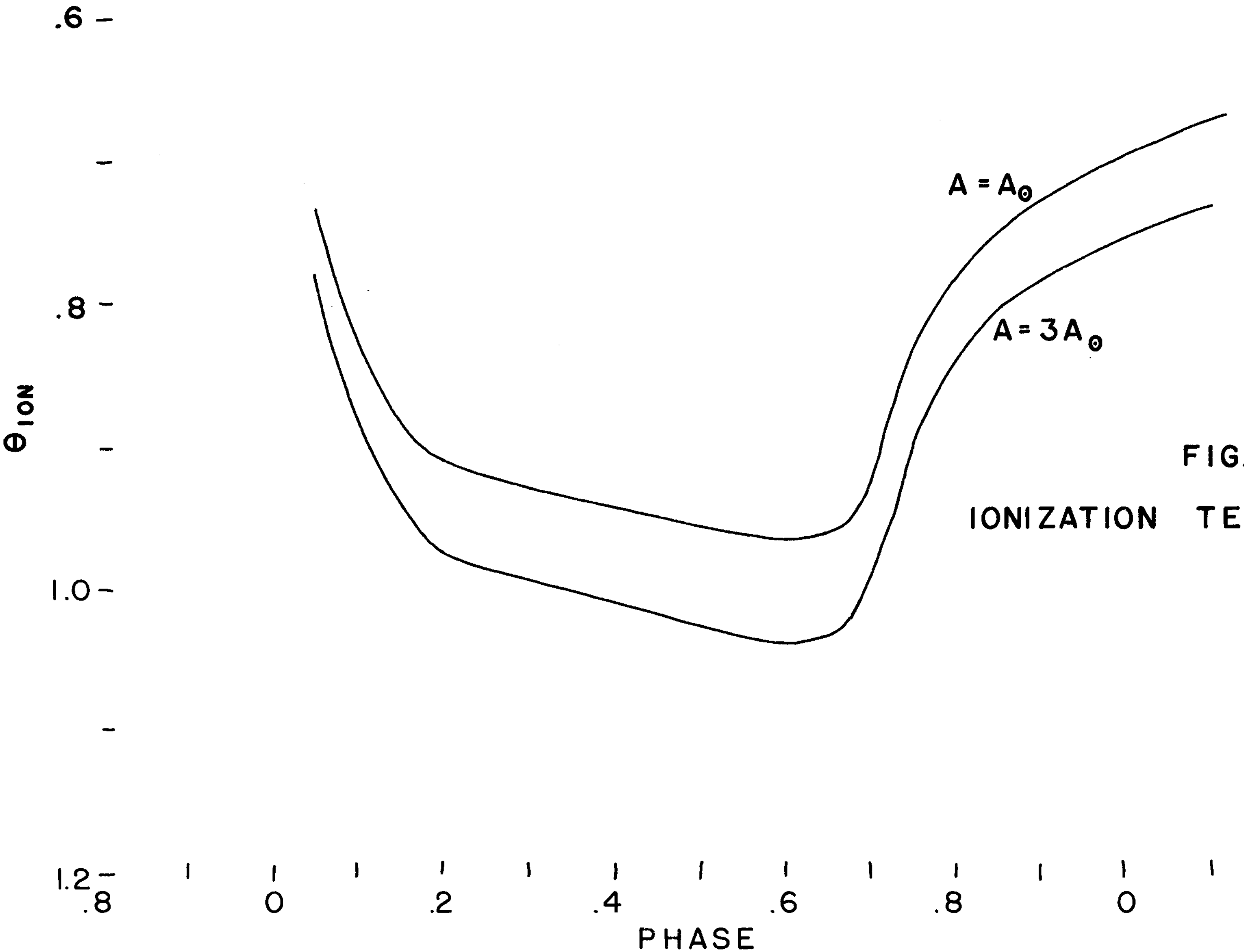

FIG. 16

IONIZATION TEMPERATURES

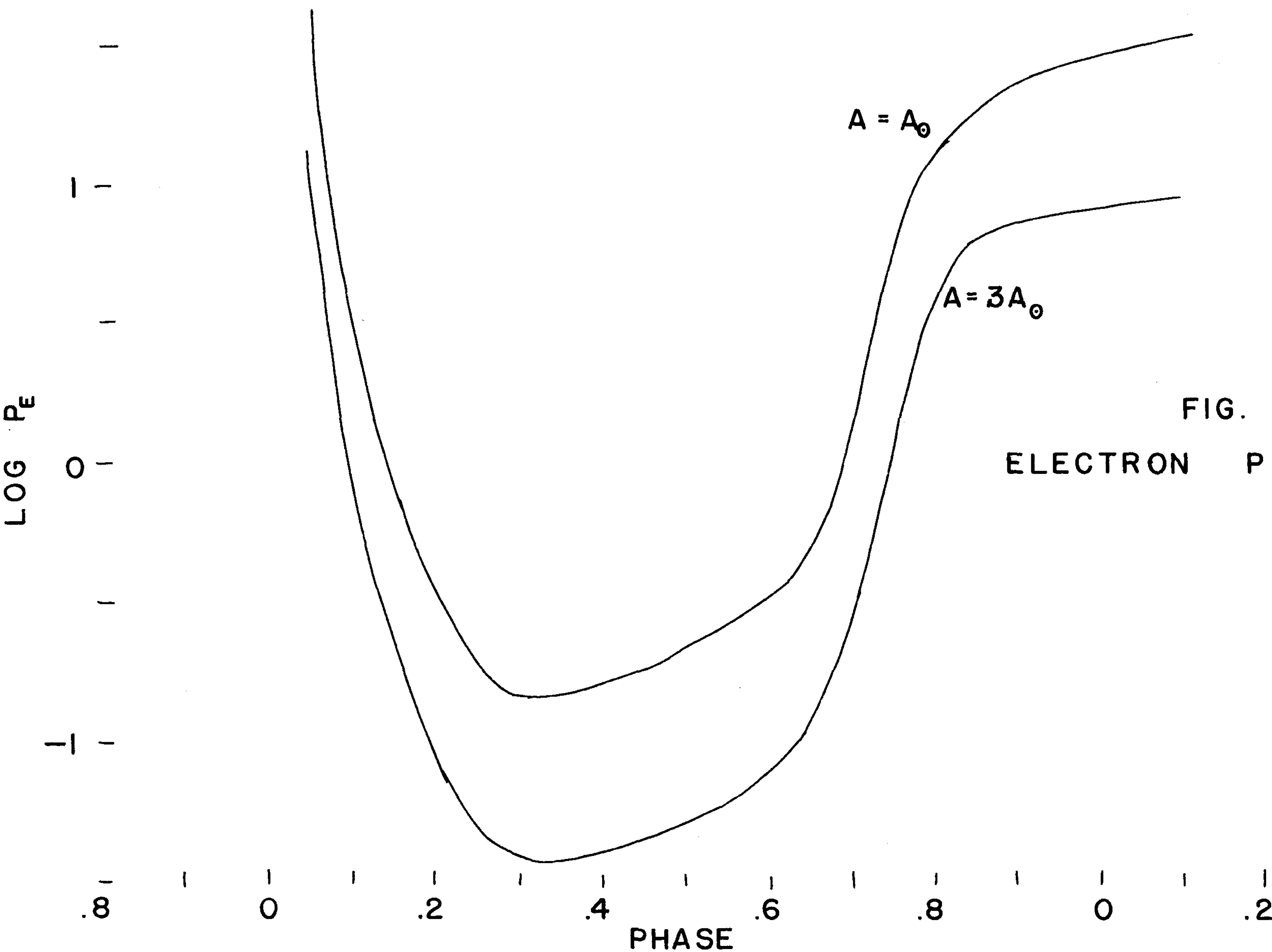

FIG. 17

ELECTRON PRESSURES

$\log P_e = -0.78$. These figures are based on the assumption that W Vir has the same Ca and Fe abundance as the sun. The agreement is probably as good as could be expected for the probable stratification for the very strong Ca K line and the moderately weak Fe lines.

6) Excitation Temperatures for MgII

To check on the large differences between θ_{ex} and θ_{ion} for Fe, excitation temperatures were derived for two high EP lines of MgII. These lines also happen to be non-metastable, unlike most of the FeI lines. To obtain θ_{ex}(MgII) it was necessary to assume an abundance for Mg so that the number of atoms in the ground state would be known. The same abundance of Mg as in α Per[12] was assumed, and calculations showed that in both α Per and W Vir practically all Mg and Fe are in the form of MgII and FeII. Then for equal abundances I assumed

$$\log\left[\frac{(N'/k)_\alpha}{(N'/k)_W}\right]_{Mg} = \log\left[\frac{(N'/k)_\alpha}{(N'/k)_W}\right]_{Fe} \qquad (18)$$

Then

$$\log\left(\eta_0 \frac{v}{c}\right)_\alpha - \log\left(\eta_0 \frac{v}{c}\right)_W = \log\left[\frac{(N'/k)_\alpha}{(N'/k)_W}\right]_{Fe} - (\theta_\alpha - \theta_W)_{ex}\chi \qquad (19)$$

where $\log(\eta_0)_\alpha = 2.93, 0.25$ for MgII 4481, 4428 respectively on our scale of f-values; also $\log(v/c)_\alpha = -4.68$ and $(\theta_\alpha)_{ex} = 0.98$, according to Greenstein[12]. Since the two lines have very high EP for their lower levels (8.82 and 9.95 ev.) the derived $\theta_{ex} = \frac{\Delta \log \eta_0}{EP}$ is rather insensitive to errors in $\log \eta_0$. Table 9 gives the excitation temperatures for MgII in W Vir; these are plotted in Fig. 18 . It is seen that the θ_{ex} for the non-metastable levels of MgII fall between θ_{ion} and $\theta_{e}x$ for FeI.

Table 9

Excitation Temperatures for MgII

Plate	Comp.	Phase	λ / EP	4481 / 8.82 ev / θ_{ex}	4428 / 9.95 ev / θ_{ex}	mean / θ_{ex}
Ce 5058		.358		1.10	1.06	1.08
5110		.650		1.20		1.20
5616	longward	.981		1.07	.95	1.01
5617	longward	.042		1.10		1.10
	shortward			.88		.88
5618	longward	.097		1.04		1.04
	shortward			1.03	.96	1.00
7013		.452		1.16		1.16
7085		.767		1.15	.95	1.05
7091	longward	.825		1.05		1.05
7102	shortward	.030		.89		.89

FIG. 18

EXCITATION TEMPERATURES

MG II

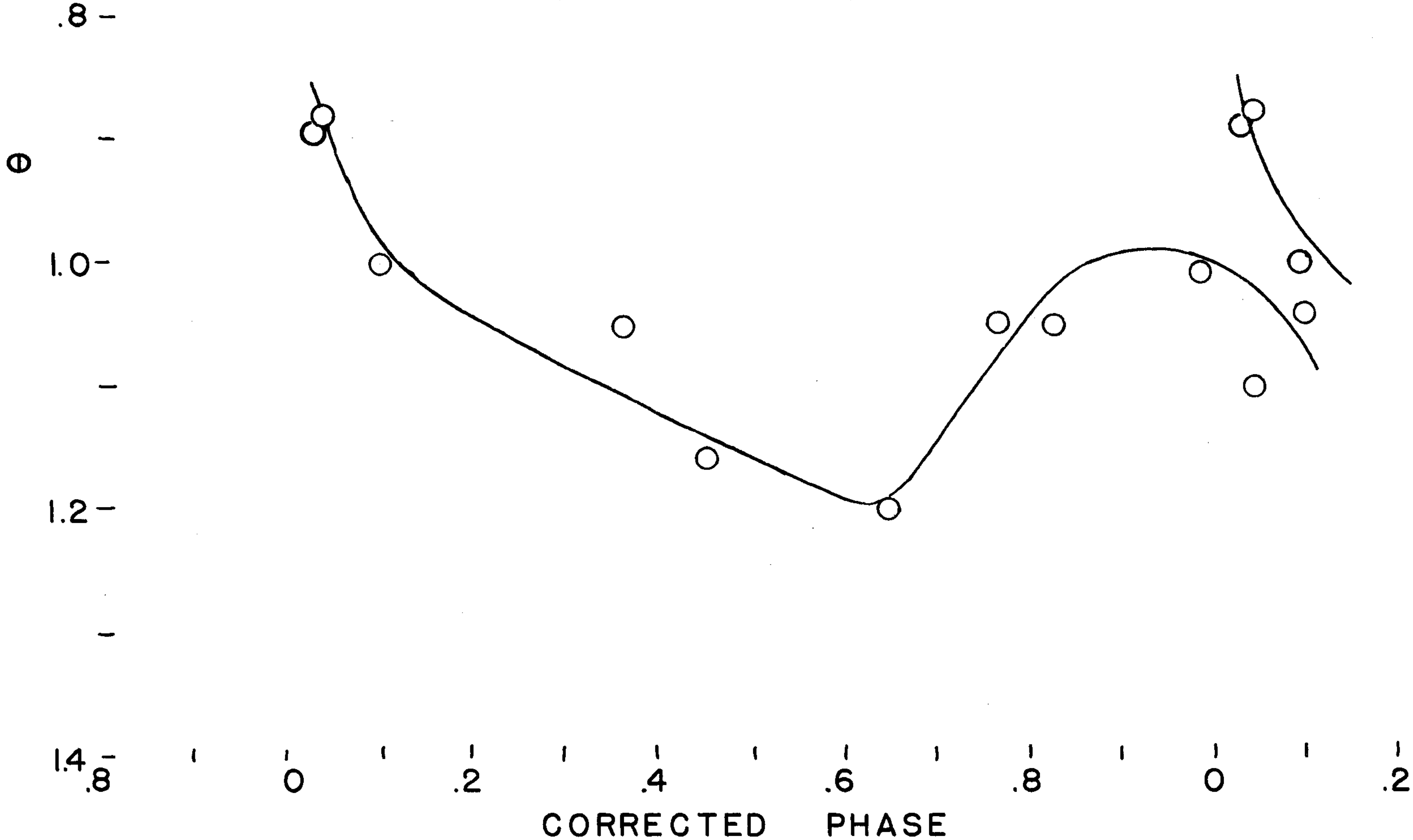

IV. Photometric Reductions

A. Conversion of Colors to Effective Temperatures

In converting from colors, C_p, to effective temperatures, T_e, it would be convenient to use the six-color photometryof 238 stars by Stebbins and Whitford[19]. First, the C_p (photoelectric) color scale was found[20] to coincide with the international color scale, C_{int}. The international color scale is based on the colors of nine North Polar Sequence stars[21]. Stebbins and Whitford[19] give C_{int} and the broad base line color V-I (violet minus infra red colors for λ_{eff} = 4220 Å, 10,300 Å) for these nine stars plus others. A least squares solution straight line gives:

$$V - I = -1.582 \pm 0.157 + 2.744\, C_{int} \qquad (20)$$

The values of V - I are listed in Table 10 for the color curve of Fig. 5 . Then using their relation between V - I and spectral class[19], the spectral classes given in Table 10 have been derived.

To convert from colors V-I to temperatures we must choose between Stebbins and Whitford's T_1 and T_2 scales. The T_1 scale is based on T_1 = 6000° for dG0; for dG2 like the sun, T_1 = 5800°. The T_2 scale is based on T_2 = 6700° for dG2. Since the effective temperature of the sun is 5713° and the color temperature, T_c, is 6500°, it appears that the T_2 scale is much closer to the T_c scale for stars of temperatures near to the sun. This relation, $T_2 = T_c$, will be incorrect for early type stars. So in Table 10 we convert from V-I to $T_c = T_2$, using the data in columns 2 and 3 of Table 11 which were taken from Stebbins and Whitford's paper[19]. Next, to convert T_c to effective temperatures, $T_e = \frac{5040}{\theta_e}$, we will use the (θ_c, θ_e) relation derived by Chandrasekhar and Münch[16], taking into consideration H^- opacity. In Table 5 and Fig. 2 of their paper they relate

Table 10

Effective Temperatures

Phase	C_p	V-I	Sp.	T_2=T_c	θ_c	θ_e
.00	.34	- .65	F4	8040	.627	.760
.05	.42	- .53	F5	7650	.659	.773
.10	.48	- .26	cF7	6860	.734	.843
.15	.54	- .10	cF7.5	6480	.777	.881
.20	.60	.07	cF8	6150	.819	.923
.25	.66	.23	cG0	5890	.856	.966
.30	.72	.40	cG1	5630	.895	1.020
.35	.78	.56	cG2	5400	.933	1.075
.40	.85	.75	cG3	5140	.980	1.157
.45	.90	.89	cG4	4970	1.012	1.190
.50	.96	1.06	cG5	4770	1.055	1.253
.55	1.00	1.17	cG6	4660	1.080	1.290
.60	.98	1.11	cG6	4720	1.067	1.270
.65	.93	.97	cG4.5	4870	1.034	1.242
.70	.86	.78	cG3.5	5100	.988	1.155
.75	.78	.56	cG2	5400	.933	1.075
.80	.66	.23	cG0	5890	.856	.966
.85	.50	- .21	cF7	6750	.747	.855
.90	.29	- .78	F3	8500	.593	.737
.95	.27	- .84	F2	8720	.578	.726
1.00	.34	- .65	F4	8040	.627	.760

Table 11

Conversions of Colors

Stebbins & Whitford					Chandra. & Münch		Keenan & Morgan	
C_p	V-I (giants)	$T_2=T_c$	θ_c	Sp	θ_e	T_e	θ_e(Ib)	T_e
.10	-1.30	11200	.450	A5	.645	7800	.579	8700
.24	- .92	9000	.560	F0	.715	7050	.664	7600
.39	- .52	7600	.663	F5	.787	6400	.813	6200
.685	.30	5780	.871	G0	.987	5100	1.008	5000
.94	1.00	4830	1.042	G5	1.234	4080	1.175	4290
1.19	1.68	4180	1.204	K0				

θ_c and θ_e for various electron pressures. It will be seen that for $\theta_e > 0.8$ the relation is independent of P_e; for smaller θ_e we will assume $P_e = 10$, which is about right for phases when the temperatures are high (see Table 8 of this paper). The final effective temperatures are plotted in Fig. 19 .

On the other hand, Keenan and Morgan[22] have correlated data on effective temperatures and spectral types with the best data available at present. Using their (spectral type, T_e) correlation, we obtain the effective temperatures in the last column of Table 11 from the spectral types in the fifth column. In the range from F2 to G6 the agreement between the empirical Keenan and Morgan and the theoretical Chandrasekhar and Münch effective temperatures is good to within 200°, which is adequate. The probable

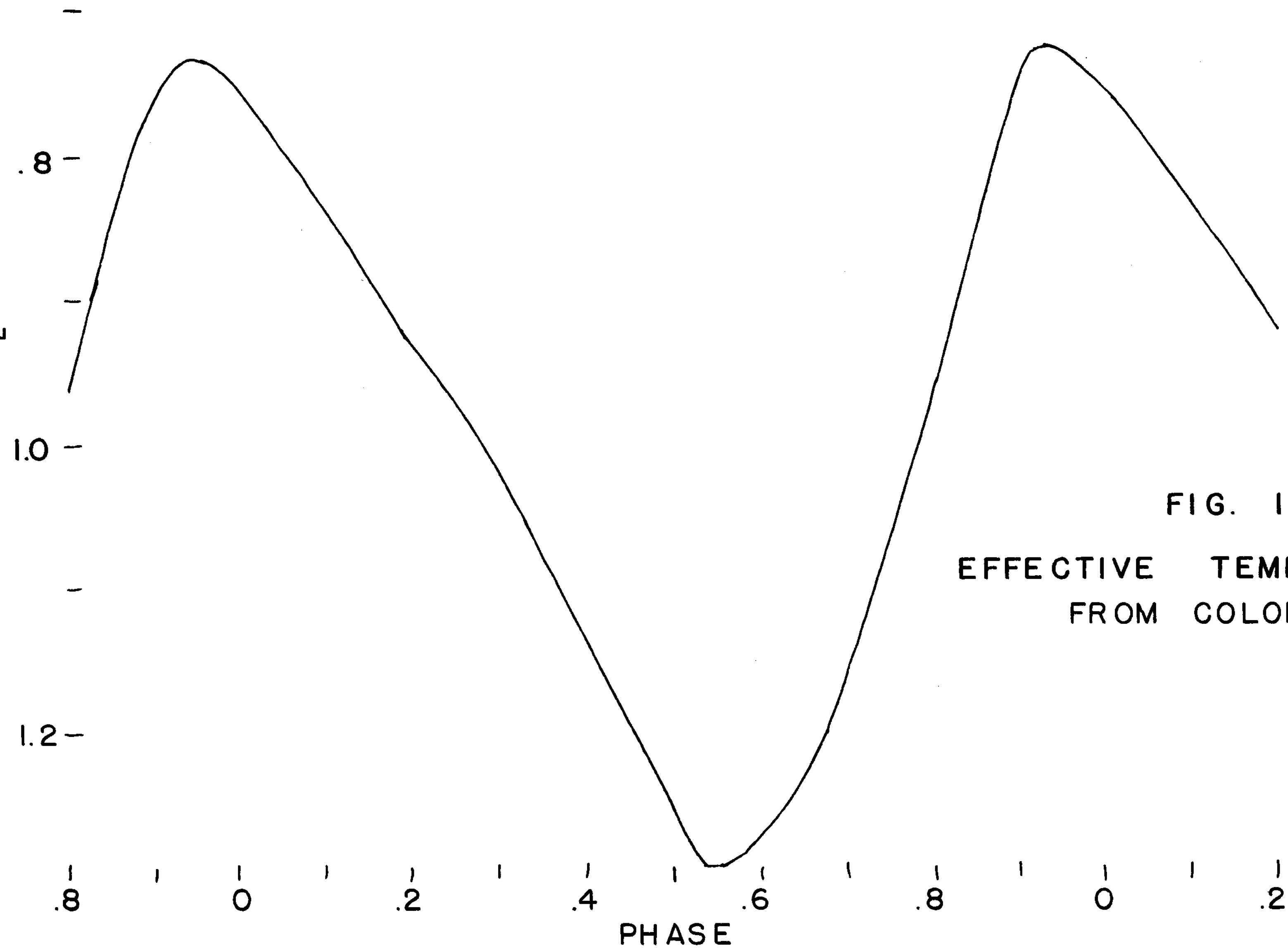

FIG. 19

EFFECTIVE TEMPERATURES FROM COLORS

error of $\pm 0\overset{m}{.}02$ in the colors, C_p, corresponds to a probable error of about 100° in the temperatures. The probable error in the excitation temperatures for FeI is about 150 to 300°. The spectral classes from the colors agree to within one or two tenths of a class with Eggen's correlation[23] of C_p with spectral class for stars of luminosity class Ib.

B. Relative Luminosities

Using the spectral types derived from the colors (Table 10), we can obtain empirical bolometric corrections from G.P. Kuiper's paper[24]. Table 12 gives the following: m_{5000} (Gordon-Kron light curve with m_{4260} at maximum = 9.9); C_p (Fig. 5); m_{5450} ($= m_{5000} - \frac{5450-5000}{5280-4260} C_p$ = photovisual magnitude); bolometric correction, B.C.; and, m_{bol}. Then from the apparent bolometric magnitudes, m_{bol}, we can obtain relative luminosities from

$$m_{min} - m = \frac{5}{2} \log \frac{L}{L_{min}} , \tag{21}$$

where the subscripts refer to minimum photographic light.

Table 12

Relative Luminosities and Radii

Phase	m_{5000}	C_p	m_{5450}	B.C.	m_{bol}	L/L_{min}	R/R_{max}
.00	9.70	.34	9.55	- .07	9.48	1.644	.384
.05	9.74	.42	9.55	- .11	9.44	1.706	.404
.10	9.78	.48	9.57	- .22	9.35	1.854	.502
.15	9.80	.54	9.56	- .25	9.31	1.923	.558
.20	9.85	.60	9.59	- .28	9.31	1.923	.613
.25	9.89	.66	9.60	- .42	9.18	2.168	.712
.30	9.94	.72	9.62	- .48	9.14	2.249	.809
.35	10.01	.78	9.67	- .52	9.15	2.228	.893
.40	10.17	.85	9.80	- .57	9.23	2.070	1.000
.45	10.41	.90	10.01	- .60	9.41	1.754	.972
.50	10.66	.96	10.24	- .65	9.59	1.486	.992
.55	10.90	1.00	10.46	- .69	9.77	1.259	.968
.60	11.07	.98	10.64	- .69	9.95	1.067	.863
.65	11.06	.93	10.65	- .63	10.02	1.000	.801
.70	10.88	.86	10.50	- .59	9.91	1.107	.727
.75	10.70	.78	10.36	- .52	9.84	1.180	.650
.80	10.49	.66	10.20	- .42	9.78	1.247	.540
.85	10.29	.50	10.09	- .22	9.87	1.148	.406
.90	10.06	.29	9.93	- .05	9.88	1.138	.301
.95	9.84	.27	9.72	- .01	9.71	1.330	.315
1.00	9.70	.34	9.55	- .07	9.48	1.644	.384

The relative luminosities are given in Table 12 and are plotted in Fig. 20 . The data would indicate that maximum luminosity occurs 0.3 period after maximum photographic light but that minimum light is independent of color. It is not known how much of the structure in the luminosity curve just after minimum is real.

C. Relative Radii

The total energy output of a star can be represented by

$$L = CR^2T_e^{\,4} , \qquad (22)$$

where C is a constant and R^2 is proportional to the area. We have relative luminosities (Table 12), so that with a knowledge of T_e as a function of phase, we can obtain relative radii. It was decided that the effective temperatures derived from colors would be the more appropriate quantities to compare with the luminosities than effective temperatures derived from ionization or excitation temperatures. From θ_e in Table 10, relative luminosities in Table 12, and eq. 22, we derive r/r_{max} as given in Table 12 and plotted in Fig. 21. From Table 12 we conclude that the radius must change by a very considerable amount to explain the observed light and color changes. The minimum radius is only a third of the maximum radius. Maximum and minimum radius are reached just before (phases 0.475 and 0.925) minimum and maximum light (phases 0.65 and 0.00) respectively. In Fig. 21 we have

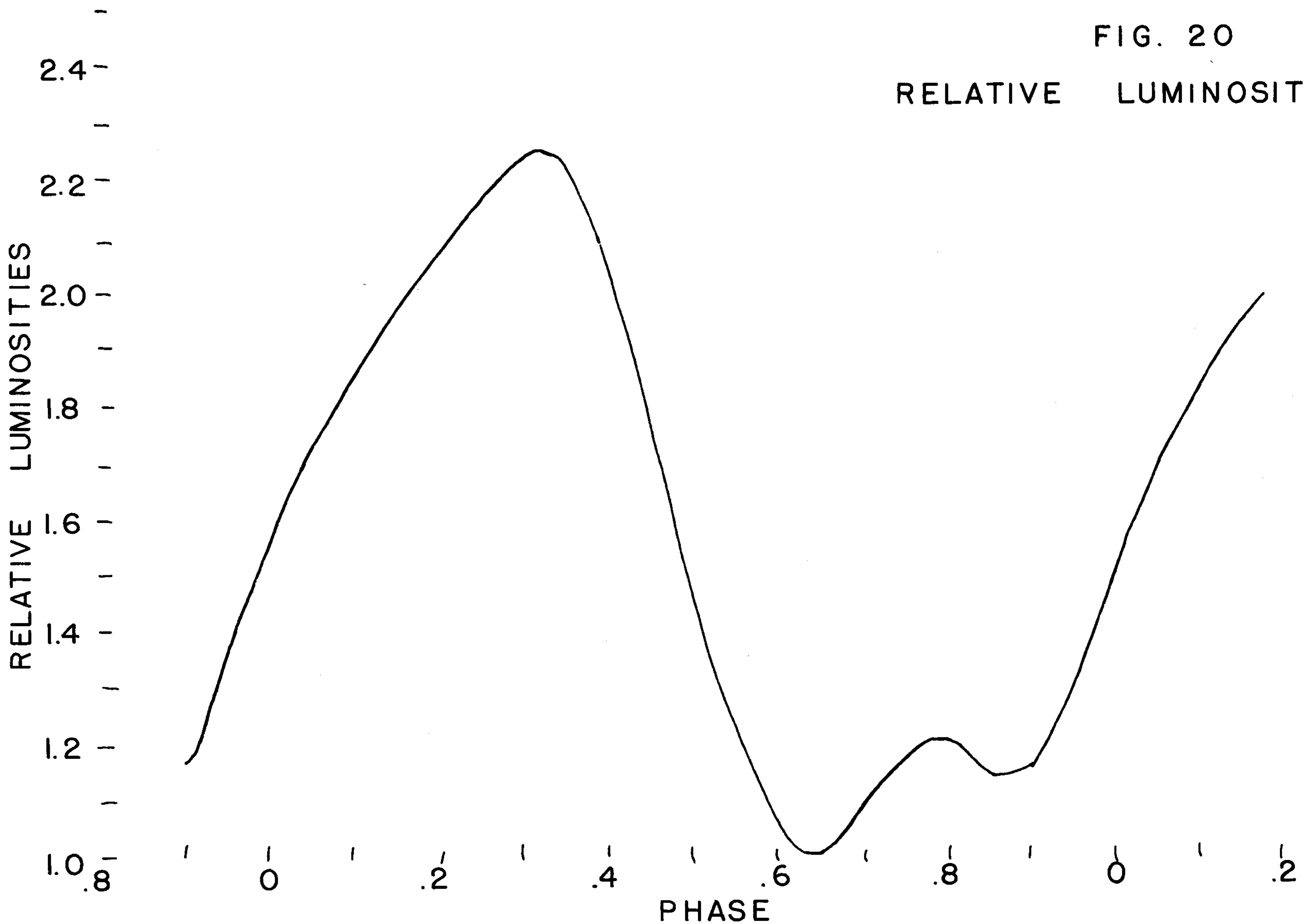

FIG. 20

RELATIVE LUMINOSITIES

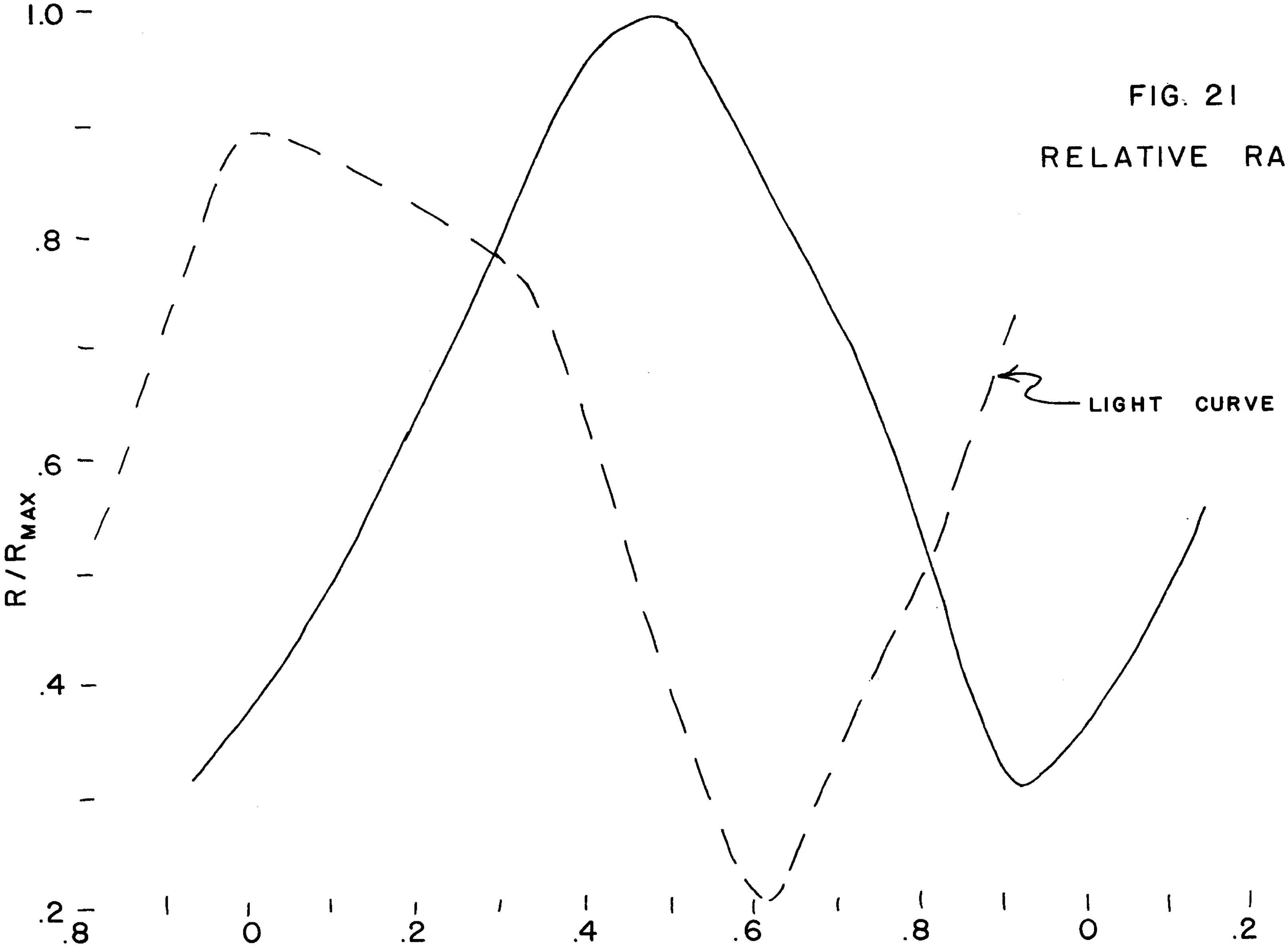

FIG. 21
RELATIVE RADII

sketched in the light curve as a dashed line. We see that the expansion lags behind the temperature changes by $\frac{1}{4}$ period as it does in Cepheids.

V. Radial Velocity Curve Reductions

By integrating the radial velocity curve over time we can find displacements of the atmosphere in kilometers as a function of phase. However, to do this we must first answer one question: What is the radial velocity of the star itself? For a Cepheid the radial velocity curve is continuous and the velocity of the star can be taken as the time average velocity of the atmosphere. In W Vir, if the motions of atoms in the atmosphere are predominantly outward or inward, the mean velocity of these atoms over one period would not be the same as the velocity of the core of the star. The mean velocity over ohases 0.0 to 1.0 is - 64.4 km./sec.; this velocity is reached at phase 0.475 . For a predominantly outward (or inward) motion, the velocity of the atmosphere will coincide with that of the star at a later (or earlier) phase. However, the phase when the maximum expansion of the photosphere (see Fig. 21) is attained is probably a time when the atmosphere has no outward or inward motion (providing there is no phase lag between the regions where the lines and continuous spectrum are predominantly produced). Fig. 21 gives a maximum radius at about phase 0.48, in good agreement with the assumption of no predominantly inward or outward motion. However, as we will see shortly, there may be some question in combining Fig. 21 with the radial velocity measurements. So for completeness we will consider all three possible mean velocities, e.g. $\rho_0 = -59.0$ km./sec. (reached at phase 0.535); $\rho_0 = -64.4$ (reached at phase 0.475); and, $\rho_0 = -68.0$ (phase 0.425).

The velocity $\rho_0 - \rho$ is not the velocity of atoms in the atmospheresince we observe only the integrated flux from the star, i.e. we see not only the atoms at the sub-solar point whose total radial motion (v_r along a radius of the star) appears as a radial velocity, but also atoms near the limb whose radial motion, v_r, is nearly pærpendicular to our line of sight. The net effect is to produce lines that are broadened from a velocity position ρ_0 to ρ, and with a maximum absorption at some velocity position in between that depends on the limb darkening. If we let $I(0,\theta)$ be the flux emitted per unit area at the stellar boundary ($\tau = 0$) and at an angle θ with the normal to the surface, then the limb darkening can be expressed by

$$I(0,\theta) = I(0,0)\left[1 - \alpha(1 - \cos\theta)\right], \tag{23}$$

where α is the coefficient of limb darkening and varies between 0 and 1. Then if $v_r \cos\theta$ is the projection of the surface velocity at a point on the line of sight and $\cos\theta \, d\omega = 2\pi \sin\theta \cos\theta \, d\theta$ is the projected surface element, the observed radial velocity is

$$\rho_0 - \rho = \frac{\iint v_r \cos\theta \, I(0,\theta) \cos\theta \, d\omega}{\iint I(0,\theta) \cos\theta \, d\omega} \tag{24}$$

Upon integration,

$$\rho_0 - \rho = \frac{4 - \alpha}{6 - 2\alpha} v_r \qquad (25)$$

For the complete range of α, the coefficient of v_r varies from 16/24 to 18/24 . With sufficient accuracy we may assume that $\alpha = 3/5$, which gives

$$v_r = \frac{24}{17} (\rho_0 - \rho) \qquad (26)$$

For each of the three assumed mean velocities, I have converted the observed radial velocities to surface velocities by means of eq. 26 . Then integrating the v_r over time, we obtain the displacements. In Table 13 we give the smoothed radial velocity curve, ρ , for the absorption lines and the displacements computed on the three assumptions of mean radial velocity. The displacements are plotted in Fig. 22 .

Next let us consider the velocities of the hydrogen emission lines. It was found that when H emission lines (Balmer series Hα through Hδ) and double emission lines occur in the same spectrum, the velocities of the H emission lines correspond to that of the shortward, or new, absorption line components (see Table 1). The velocities given in Table 1 were measured by Sanford on the original plates. They need correction since a sharp narrow absorption line is superimposed on each broad emission line; Sanford measured only the strongest peak of the remaining bisected

Table 13

Displacements from Radial Velocities

Source	Phase	ρ	$(r_{max}-r)$ in 10^6 km. for r_{max} at phase:		
			0.535	0.475	0.425
				36.70	
emission lines	0.65	- 74.7			
				35,62	
	.70	78.2			
				34.16	
	.75	81.9			
				32.32	
	.80	85.5			
				30.10	
	.85	89.1			
				27.50	
	.90	92.4			
			31.15	24.55	20.53
absorption lines	.95	95.2			
			27.33	21.31	17.66
	.00	96.4			
			23.39	17.93	14.67
	.05	96.2			
			19.48	14.59	11.70
	.10	94.9			
			15.69	11.37	8.87
	.15	92.2			
			12.20	8.45	6.32
	.20	88.6			
			9.08	5.90	4.15
	.25	84.5			
			6.39	3.78	2.41
	.30	80.2			
			4.16	2.12	1.13
	.35	75.7			
			2.40	.93	.32
	.40	71.0			
			1.14	.23	.00
	.45	66.6			
			.34	.00	.15
	.50	62.2			
			.00	.23	.76
	.55	58.0			
			.10	.91	1.81
	.60	-54.0			
			.63	2.00	3.29

Table 13 (cont.)

.65	-50.3			
		1.55	3.49	5.15
.70	46.7			
		2.84	5.35	7.39
.75	43.5			
		4.47	7.55	9.97
.80	40.8			
		6.39	10.04	12.84
.85	38.7			
		8.53	12.74	15.92
.90	37.5			
		10.79	15.58	19.14
.95	38.0			
		13.01	18.36	22.30
1.00	40.0			
		15.01	20.93	25.24
1.05	43.0			
		16.69	23.18	27.88
1.10	-46.5			
		18.01	25.07	30.14

emission line.

To improve the H emission line velocities, I made use of the available spectrophotometer tracings. For each line the profile of the emission line (minus the absorption component) was sketched in. The position of the center of this emission line was compared with that of the hydrogen absorption line whose velocity is known (see Table 1). The values of ρ_{em} are given in Table 14 along with the estimated weights of the determinations in parenthesis. These velocities were plotted with squares in Fig. 1, with relative sizes of the squares representing the relative weights.

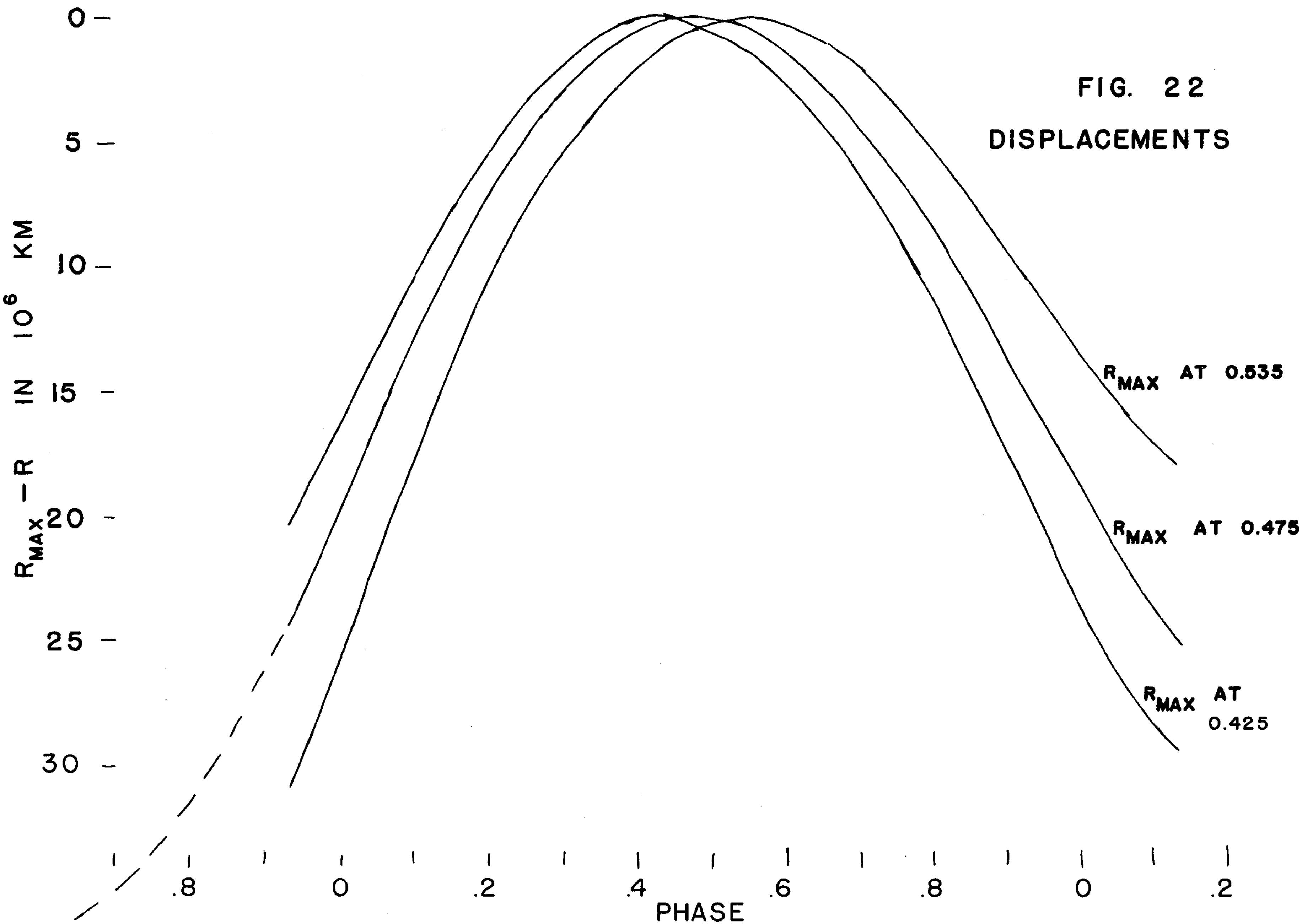

FIG. 22

DISPLACEMENTS

Table 14

Velocities of Hydrogen Emission Lines

Plate	Phase	$(\rho_{em} - \rho_{abs})$ in km/sec and wt.				ρ_{em}
		$H\delta$	$H\gamma$	$H\beta$	$H\alpha$	
Ce 5110	.650	- 5.7(2)	-20.4(1)		-16.0(3)	-78.7(6)
7080	.709	-20.5(2)		-11.7(3)		-78.8(5)
7085	.767	-36.6(2)		-29.0(3)		-79.8(5)
7091	.825	-41.0(3)		-44.3(3)		-84.9(6)
5616	.981	-34.4(1)				-73.0(1)
7102	.030	-56.3(1)	-56.7(1)			-96.7(2)
5617	.042	-30.0(1)				-70.1(1)
6211	.089		-47.0(1)			-85.5(1)
5618	.097		-40.1(1)	-46.1(1)		-85.5(2)

If we now accept the coincidence of the region where the H emission lines are formed with the region of formation of the new wave absorption lines, we can trace the motion of the new wave back to earlier phases since the emission lines occur about 0.3 period earlier than the absorption lines of the new wave.

To substantiate this assumption we will investigate the relative positions of the regions where the H emission lines are formed and where the H absorption lines are formed. The latter have very closely the same velocities as the longward (old wave) metallic absorption lines (see Table 1), and hence we can assume that these two sets of lines are formed at the same atmospheric depth. We wish to find out whether the emission lines are formed high in the atmosphere, or (as we suspect) below the old wave in the region of the new wave. A study of the depth of the $H\delta$ absorption line on plate

Ce 5617 shows definately that it was formed above the emission line. Hence we have more confidence in the assumption of the previous paragraph.

The smoothed velocity curve for the emission lines is given at the top of Table 13 . The displacements have been calculated for r_{max} at phase 0.475 and are plotted as the dashed curve in Fig. 22 .

VI. Chronology of Events

A. Observational

In this section we will merely collect the observed facts, heretofore presented, into a chronological sequence. In the following section we will give possible models or explanations for the observed phenonema. We choose to start the description with the appearance of the emissiom lines at minimum light and we will carry it through nearly two cycles.

At about minimum light (phase 0.65), when the absorption lines are strong, there appear hydrogen emission lines of the Balmer series with an outward surface velocity of 20 km./sec. They rapidly increase in strength and also accelerate outward to a maximum surface velocity of 45 km./sec. At the same time the absorption lines are rapidly decreasing in strength. Then at about phase 0.90 a new set of absorption lines appears with the same outward surface velocity as the emission lines. These new (shortward) absorption lines rapidly increase in strength while the emission lines and older (longward) absorption lines gradually fade. The new absorption lines start out with a high excitation temperature (5400°) but one that is dropping rapidly. They also indicate a relatively low Doppler velocity (5 km./sec.) and a large outward surface velocity (45 km./sec.).

At maximum light the two sets of absorption lines are of about equal strength except for differences due to different ionization and excitation temperatures. The hydrogen lines show a weak emission component with a velocity like that of the new metallic absorption lines and a weak absorption component with a velocity like that of the old metallic absorption lines. The region forming the emission component lies below that forming the absorption component. At this phase during most cycles a very broad, shallow hydrogen absorption line is also present (see Fig. 2). The large width of this line may be due to either Stark broadening , like H lines in A stars, or to a very large thermal broadening. If due to Stark broadening, the line width indicates a P_e/T ratio of the order of magnitude as for A-type main sequence stars (about 10^3 dynes/cm^2 / 10,000°). If due to pure thermal broadening, we derive a temperature of 30×10^6 deg. The line has a velocity like that of the emission line.

As we progress to phase 0.10, the H emission lines and the older metallic absorption lines disappear. The new absorption lines are nearly up to full strength. Since the temperature is still dropping rapidly while the degree of ionization remains almost constant, we conclude that the electron pressure is also dropping rapidly (by a factor of 300; see Fig. 17). The motion is still outward but a deceleration is starting. However, the displacements are very large (see Fig. 22).

The expansion gradually slows down and ceases at around phase 0.475, after a displacement of about 36×10^6 km. This is when the electron pressure (and presumably the total pressure) is smallest (of the order of 0.1 dynes/cm^2). Also the opacity is at a minimum so the lines are strongest. The various temperatures all show nearly a minimum, but the excitation temperatures have gone through a much larger range than the ionization temperatures. The colors are very red.

Minimum photographic light and excitation and ionization temperatures occur (phase 0.65) a little after maximum expansion. The luminosity curve shows a general minimum from phase 0.65 to 0.90 with fluctuations that may not be real. The Doppler velocity is still increasing (9 km./sec.) and continues to do so throughout the contraction. The velocity of contraction increases until about phase 0.8 . Around phase 0.7 there is a rapid increase in temperature, electron pressure, and opacity. The lines fade in strength.

However, already at phase 0.65 another set of emission lines, with the same characteristics as the previous set, has started and at about phase 0.90 a new set of weak absorption lines appears. We must now call these the new lines and the previous ones (which were called the new lines one cycle before) will now be called the old set. We will not repeat the characteristics of this new set but will now focus our attention on the old set that we have been following and the differences between the two.

The excitation temperatures for FeI and MgII show a maximum at phase 0.9 and then a drop. The ionization temperatures do not show a drop, but gradually rise after phase 0.9 . However the ionization temperatures during phases of double lines are of doubtful value because of the composite nature of the spectrum. The FeI excitation temperatures are 800 to 1000° lower for the older lines than for the newer ones at the same time. Similar results are derived for MgII but not for the (incorrect) ionization temperatures. The Doppler velocities reach a maximum of 12 km./sec. for the older lines while the newer ones at the same time have a velocity of 5 km./sec. The displacements of the regions causing the new and old lines depends greatly on the assumed star velocity; for the best value (r_{max} = 0.475) the displacements are the same at phase 0.00, indicating that at phase 0.00 the atoms moving upward pass the ones moving downward. This is also just the phase when the two sets of lines are apparently equal in strength.

The old lines disappear at about phase 0.10 . Hence the whole cycle of events extends for about 1.45 periods rather than just one period. It should be noted that the ranges in electron pressure, opacity, temperature, displacement, and other variables is much larger than for most Cepheids.

Normally in Cepheids the relative expansion derived from the luminosity law is fitted to the displacement curve derived from the radial velocity curve to calibrate the scale of the changes. This then leads to the radii of the star (in kilometers) and then to absolute luminosities. When this was tried with W Vir (using Figs 21 and 22), the maximum radius was found to be $22x10^6$ km. However, the total displacement is $36x10^6$ km., so the result is absurd. We conclude that the curves cannot be combined; this may be because the derived data may be for different atmospheric depths that have different motions. Assuming a luminosity from the period-luminosity relation for the Cepheids and effective temperatures from colors, we derived a maximum radius of $66x10^6$ km.

B. Interpretation and Discussion

Adiabatic pulsations of a bounded atmosphere require the density, temperature, pressure, and negative displacement curves to be exactly in phase. Since these are not all strictly in phase in W Vir, it is not likely that the phenomena involved can be explained by a standing wave. Investigations by Eddington, Schwarzschild, Reesinck, and others (see ref. 25, page 87) show that the lack of a sharp boundary to an atmosphere is insufficient to cause the observed phase lags.

However, any dissipation of energy in the atmosphere will lead to phase differences. Many of the features of the pulsation in Cepheids can be explained in terms of a progressive, or running, wave, although quantitative tests have been unsuccessful so far (ref. 25, page 94). Furthermore, it will be necessary to consider anharmonic pulsations to explain the non-sinusoidal variations of the physical parameters.

A quantitative analysis of W Vir by progressive waves is hindered at present by a lack of good data on absolute dimensions and luminosity. For the time being we can give only a qualitative picture of the phenomena. Let us suppose that the expansionphase of a progressive wave starts outward from some unknown depth. While still compressed the density, pressure, and temperature are high, but as the expansion wave moves outward, the three parameters must decrease and reach a minimum when the displacement has reached the amplitude of the pulsation. If the opacity is sufficiently small, it will be possible to see a new expansion wave coming up from a lower depth while the upper part of the atmosphere is just beginning to contract. The simultaneous appearance of two regions, one of which is moving inward and the other outward, indicates a phase difference of about 180° between two layers of the atmosphere.

I will not elaborate more on this model since its detailed application to W Vir needs a considerably ~~more~~ greater amount of work. However, at present I will record several interesting aspects and some objections to this picture.

The colors give effective temperatures that are much lower than the ionization temperatures at maximum expansion but that agree at minimum radius. A color-spectrum difference (K2 and G1 at r_{max}) may be due to a totally different model atmosphere which would make our conversion of colors to temperatures on the basis of normal stars entirely incorrect. However, we are tempted to suggest that this difference may be due to an extended atmosphere, particularly at maximum radius. A similar color-spectrum difference has been observed in novae and other expanding stars. The theory of extended atmospheres has been developed by Kosirev[26] and Chandrasekhar[27,28] and applied to Nova Herculis by Whipple and

C.P. Gaposhkin[29]. Difficulties were encountered when this theory was applied to W Vir because of a lack of a model atmosphere.

A second point of interest is the large range in the different kinds of temperatures at any one phase. In Fig. 23 we have plotted the smooth curves from Figs. 10,16, 18, and 19 . The excitation and ionization temperature curves are somewhat similar in shape but differ in amplitude. In a normal star the temperature gradient is given[30] by:

$$T^4(\tau) = \frac{3}{4} T_e^4 \left[\tau + q(\tau) \right] \qquad (27)$$

The lines are formed at a mean depth of $\tau = 0.3$. In the sun the excitation temperature for FeI happens to coincide with T(0.1). In Table 15 we compare solar and W Vir temperature gradients.

Table 15

Temperatures in the Sun and W Vir

τ	$T(\tau)/T_e$	Sun		W Vir phase 0.3	W Vir phase 0.65
0.0	.811				
.1	.855	T_{ex}=4875	T_{ex}/T_e= .853	T_{ex}=4060	T_{ex}=3450
.3	.920	T_{ion}=5300	T_{ion}/T_e=.927	T_{ion}=5420	T_{ion}=5250
.65	1.000	T_e =5713	T_e/T_e =1.000	T_e =4940	T_e =4100
1.0	1.062				

Two reasons for the large temperature range can be given. First, departures from thermal equilibrium and dilu-

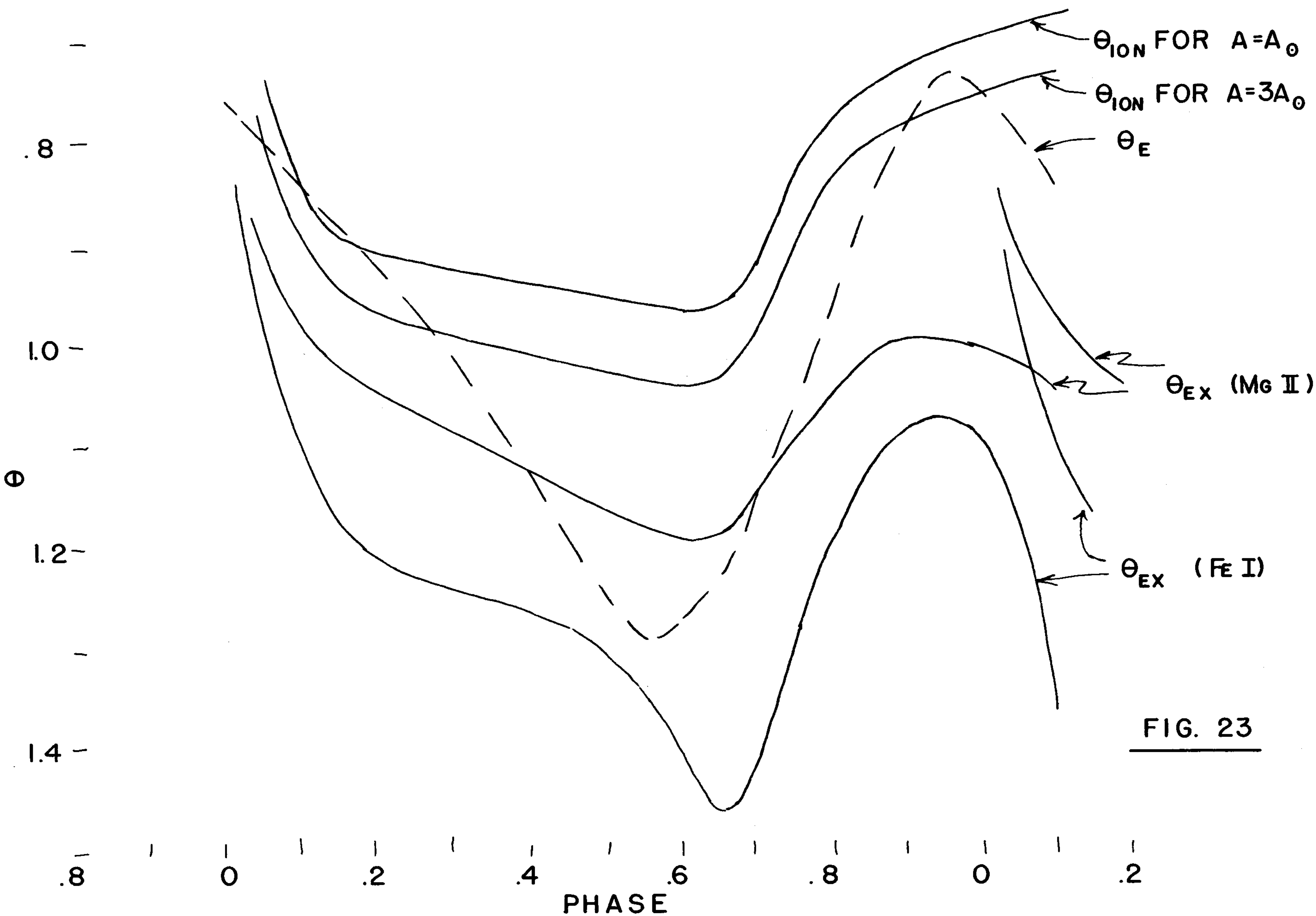

Θ
.8
1.0
1.2
1.4
PHASE
.8
0
.2
.4
.6
.8
0
.2
Θ_{ION} FOR $A = A_0$
Θ_{ION} FOR $A = 3A_0$
Θ_E
Θ_{EX} (Mg II)
Θ_{EX} (Fe I)

FIG. 23

tion of radiation may make the population of metastable FeI levels anomalous. There is some indication that stable FeI levels give higher temperatures. The second possibility is that an extended atmosphere is present, particularly at maximum radius when the temperature range is largest. An extended atmosphere has a large temperature gradient; calculations showed that it is entirely sufficient to give the large observed ranges.

A difficulty that is forseen in applying the progressive wave theory to W Vir is to explain the large differences between the two regions of the atmosphere as observed in the double lines. The FeI excitation temperatures differ by 800 to 1000° and the Doppler velocities are 5 and 12 km./sec. for the two regions. It is not likely that with continuous gradients such a range in parameters could be found within an optical depth of 1 or 2. These large differences may be indications of a real discontinuity in the atmosphere, i.e. a shock wave. Calculations will have to be made to determine whether a shock wave could be expected. We cannot observe the velocity of the shock front but only the residual velocity of flow of the material.

I have not yet done all the things possible with the present data. The line strengths during phases of double lines must be corrected for the overlying continuous spectrum. Then the corrected electron pressures will lead to total pressures and densities. Finally, the various pulsation and eruptive models must be carefully examined. It is also desirable to obtain more complete color data.

VII. References

1. A.S. Eddington : M.N.R.A.S. 101,182,1941

2. W. Baade : Publ. Univ. of Mich. Obs., Vol X : The Structure of the Galaxy, 1950

3. A.E. Joy: Ap.J. 86,363,1937

4. Morgan, Keenan, and Kellman : An Atlas of Stellar Spectra ; Univ. of Chgo. Press, 1943

5. A. Nielson : A.N. 262,422,1937

6. K.C. Gordon and G.E. Kron : Ap.J. 109,177,1949

7. C.A. Chant : H.A. 80,221,1917

8. W.H. Wrubel : Ap.J. 109,66,1949

9. R.B. King and A.S. King : Ap.J. 87,24,1938

10. W.W. Carter : Phys. Rev. 76,962,1949

11. K.O. Wright : Publ. Dom. Astrophys. Obs. VIII,#1,1948

12. J.L. Greenstein : Ap.J. 107,151,1948

13. R.B. King : Ap.J. 95,78,1942

14. J.L. Greenstein : Ap.J. 113,705,1951

15. ref. 12, page 178

16. S. Chandrasekhar and G. Münch : Ap.J. 104,446,1946

17. M. Schwarzschild, L. Spitzer, Jr., and R. Wildt : Ap.J. 114,398,1951

18. P. Wellmann : Veröff d. Sternw. Berlin-Babelsburg, Vol. 12, Part IV, 1939

19. J. Stebbins and A.E. Whitford : Ap.J. 1o2,318,1945

20. J. Stebbins, A.E. Whitford, and H.L. Johnson : Ap.J. 112,469,1950 ; Table 2

21. H.L. Johnson and W.W. Morgan : Ap.J. 114,522,1951

22. P.C. Keenan and W.W. Morgan : Astrophysics, edited by J.A. Hynek ; McGraw-Hill Book Co., 1951 ; page 18 and Table 13

23. O.J. Eggen : Ap.J. 113,663,1951

24. G.P. Kuiper : Ap.J. 88,429,1938

25. S. Rosseland : The Pulsation Theory of Variable Stars; Oxford, 1949

26. N.A. Kosirev : M.N.R.A.S. 94,430,1934

27. S. Chandrasekhar : M.N.R.A.S. 94,444,1934

28. S. Chandrasekhar : Proc. Camb. Phil. Soc. 31,145,1935

29. F.L. Whipple and C.P. Gaposhkin : Harv. Cir. 413,1936

30. S. Chandrasekhar : Ap.J. 100,76,1944 ; eq. 54.

TABLE 4

Values of -log W/λ

Plate Number, Corrected Phase, Components

Mult. No.	λ	log gfλ	5110 .650	7080 .709	7085 .766	7091 .825 l*	7091 .825 s*	5616 .981 l*	5616 .981 s*	5647 .006 l*	5647 .006 s*	7102 .030 l*	7102 .030 s*	6207 .041 l*	6207 .041 s*	5617 .044 l*	5617 .044 s*	6211 .094 l*	6211 .094 s*	5618 .099 l*	5618 .099 s*	5651 .123	5556 .198	5058 .358	7010 .401	7013 .458	7017 .516
Fe I																											
2	4347.24	- .53	4.79	5.19	5.48	5.21																5.23	5.17	4.77	4.95	5.07	5.05
	4375.93	+1.82	4.00	4.17	4.23	4.48	4.81		4.97				4.84		4.89				4.58		4.46	4.37	4.21	4.22	4.20	4.15	4.06
	4389.24	.34	4.32	4.51	5.17	5.42										5.31			5.53				4.61		4.36	4.75	4.45
	4427.31	1.87	4.00	4.02	4.13	4.59	5.07	5.21					4.67		4.67	5.61	5.04		4.42	5.07	4.49	4.34	4.21	4.17	4.07	4.11	4.06
	4489.74	.86	4.30		4.94	4.78										5.53						4.64	4.39	4.32	4.53	4.29	4.24
3	4199.97	.66	4.55	4.76	5.36	5.09									5.39	5.31			5.59			5.03	4.91	4.72	4.60	4.61	4.44
	4206.70	.99	4.23	4.39	4.54	4.86							5.11		5.31	4.92			4.94		4.69	4.49	4.34	4.24	4.48	4.31	4.21
	4216.19	1.51	4.08	4.11	4.35	4.79													4.60			4.32	4.21	4.05	3.92	4.12	4.14
3,41	4291.47	.74	4.20	4.16	4.61	5.03									5.41										4.26	4.34	
4	3824.44	2.97								4.00	4.27			4.47	3.94	4.04	4.22		3.99		4.10	3.95					
	3856.37	3.03								4.07	4.14				4.29	4.25				4.23	4.17	4.06					
	3859.91	3.61								3.99					4.08	4.32	4.52	4.71	4.05		4.24	4.11		3.81			
	3878.57	3.00								4.09					4.05	4.23	4.39		4.22	4.25		3.98					
	3886.28	3.26								4.00	4.47						4.57										
	3895.66	2.75								4.09	4.32				4.35	4.30	4.49		4.15		4.37	4.01		4.05			
	3899.71	2.87								4.05	4.40				4.27	4.19	4.35		4.06		4.42	4.18					
	3906.48	2.34													4.20				4.07		4.32						
	3920.26	2.73								4.20	4.44	4.84	4.41	4.74	4.21	4.33	4.60		4.27			4.19					3.71
	3922.91	2.84								4.28	4.52	4.75	4.37		4.23	4.40	4.56		4.14	4.36	4.22	4.27	4.10		3.78	3.81	
18	4100.74	2.10																							4.48		
	4139.93	1.44	4.55	4.54	4.97	4.85			5.24				5.62		5.34				5.16	5.71		4.69	4.52	4.55	4.57	4.50	4.45
19	4174.92	2.54	4.29	4.35		4.55									5.15		5.33		4.88		4.66	4.36	4.39		4.23	4.32	4.31
20	3820.43	4.55								3.99	4.37				4.01	4.08	4.47		4.18		4.17	3.94					
	3825.88	4.41								4.00	4.22				4.12	4.11	4.23				4.15	3.99					
	3840.44	4.01									4.59				4.39				4.13		4.22						
	3849.97	3.80								4.18	4.47				4.23	4.24	4.45				4.31	4.15					
	3865.53	3.67								4.28	4.38			4.82	4.37	4.46	4.50		4.13	4.61	4.24	4.17		4.00	3.91	3.82	
	3872.50	3.72																				4.13					
	3878.02	3.70													4.28				4.14		4.25	4.06		4.19		3.91	
	3887.05	3.50								4.36						4.57											
	3898.01	2.78						4.60	4.65						4.37			4.72	4.14		4.32	4.14		4.08	3.97	3.95	3.86
	3917.18	2.67											4.76						4.54		4.35	4.17	4.34	4.17	4.12	4.03	
21	3758.23	4.46																				4.03					
	3763.79	4.25								3.98	4.33																
	3767.19	4.15								4.11	4.26					4.21	4.46			4.03	4.21						
	3787.88	3.76								4.19	4.31				4.12	4.38	4.31		4.10	4.53	4.31	4.12					
	3795.00	3.84								4.08	4.38					4.39	4.38										
22	3786.68	2.62																	4.46			4.16					
	3790.09	3.06																	4.21	4.41	4.16						
	3812.96	3.56																	4.07			4.05					
	3814.53	2.43																				4.01					
	3850.82	3.12																	4.24			4.25		4.11	3.95	3.95	
38	4733.60	2.12																									4.53
39	4602.00	1.80			5.35																		5.39			4.75	4.72
	4602.94	3.01	4.41	4.66	4.69	5.07							4.90						4.96		5.02	4.40	4.44	4.43	4.26	4.35	4.38
	4632.91	2.35	4.87			5.15																5.06			4.54	4.60	4.46
41	4337.05	3.08						4.94											4.54			4.22		4.23	4.28	4.20	4.11
	4383.55	4.80	4.13	3.88	4.02	3.85	4.41	4.16	4.68				4.25		4.45	4.29	4.79		4.29		4.23	4.30	4.07		3.88	3.89	3.86
	4404.75	4.55	3.91	4.00	3.98	4.01	4.48	4.47	4.97			4.50	4.37	5.58	4.37	4.24	4.56	5.00	4.26	4.44	4.23	4.18	4.02	3.94	3.96	3.97	3.87
	4415.12	4.20	4.07	4.22	4.07	4.17	4.97	4.87	5.27			5.33	4.36		4.49		4.62		4.24		4.38	4.29	4.19	4.06	4.07	4.21	4.12
42	4147.67	2.83	4.18	4.36	4.70	4.59							5.13		5.17				4.63		4.84	4.38	4.34	4.32	4.29	4.30	4.24
	4202.03	4.06	4.13	4.03	4.06	4.14	4.58	4.46	4.78			5.31	4.37		4.48	4.72	4.43		4.17		4.08	4.19	3.97	3.95	3.92	4.09	3.92
	4250.79	4.03	4.22	4.07	4.14	4.19	4.90	4.73				5.32	4.36		4.53		4.64		4.26			4.29	4.19	4.10	4.12		4.08
	4271.76	4.46	3.94		4.04	4.01		4.37	4.84			4.70	4.26		4.65	4.52	4.44		4.20	4.31	4.03	4.29	4.10	3.98	3.93	3.92	3.89
	4325.76	4.68	4.07	3.95	4.04	3.86		4.38	4.86			4.73	4.32		4.35	4.47	4.47	5.40	4.33	4.32	4.19	4.21	4.14	4.00	3.99	3.92	3.90

Mult. No.	λ	log gfλ	5110 .650	7080 .709	7085 .766	7091 .925 1*	7091 .925 s*	5616 .981 1*	5616 .981 s*	5647 .006 1*	5647 .006 s*	7102 .030 1*	7102 .030 s*	6207 .041 1*	6207 .041 s*	5617 .044 1*	5617 .044 s*	6211 .094 1*	6211 .094 s*	5618 .099 1*	5618 .099 s*	5651 .123	5556 .198	5058 .358	7010 .401	7013 .458	7017 .516
Fe I																											
422	4141.86	3.19																				5.51				5.05	
472	4517.53	3.29											6.20									5.51			5.44	5.09	5.06
476	4387.90	3.70	5.51	5.51																		5.33			5.25	5.02	4.83
476a	4182.38	3.78	4.82		5.08	4.97																	4.66		4.66	4.87	4.38
482	4248.23	4.55				5.60			4.99							5.67	5.18		5.16				4.71		4.69	4.63	4.49
	4267.83	3.85	5.09	5.24	5.50	5.50		5.34							5.12		5.20		4.93			4.94	4.58	4.73		4.66	4.52
515	4480.14	3.73		5.43	5.26	5.18							5.28									5.36	5.03		5.05	4.94	4.81
522	4199.10	5.16	4.29	4.48	4.38	4.53		5.00					4.42		4.75	4.98	4.50		4.35			4.49	4.32	4.29	4.30	4.32	4.27
523	4143.42	4.96	4.25	4.35	4.44	4.48							4.62				4.68		4.46	5.09	4.65	4.50	4.25		4.23	4.16	4.14
527	4017.16	4.28	4.58					5.49	5.26				5.06		5.01	5.15	5.11		5.11		4.77	4.75	4.44		4.46	4.43	4.46
554	4607.65	3.78	5.29	5.15	5.60	5.51							5.09									4.90	4.86		4.83	4.79	4.89
	4625.05	4.08	5.19	5.27		4.95							5.67									5.15	4.76		4.83	4.93	4.52
	4637.51	3.93																				4.95			4.93	4.96	
	4668.14	4.26																				4.91				4.62	4.75
	4707.28	4.69																									4.46
	4736.78	4.83																									4.28
555	4504.84	2.95	5.55										5.50									6.44			5.44	5.34	5.39
555,654	4022.74	3.35																									4.96
558	4070.77	4.43	4.71						5.14	5.10					5.20	4.67	4.97				5.42	4.81	4.63		4.62	4.54	4.59
	4109.07	3.48			5.39																						4.71
559	4067.98	4.80	4.54					5.51							4.79	5.60			4.65	5.35	4.80	4.65	4.44	4.32	4.40	4.34	4.57
	4085.31	4.78								5.60			4.57		4.78				4.74		4.59	4.53	4.30	4.24	4.19	4.38	4.17
597	4285.44	4.03			5.61			5.70					5.37									5.29	4.64			4.79	
655	4040.65	5.28	4.55						5.63	4.86			5.38		4.93	4.75	5.17		5.00			4.59	4.46	4.35	4.32	4.27	
689	4200.93	4.34	4.79		5.25										5.43		5.09		5.09		4.79	5.03	4.53	4.57	4.79	4.63	4.66
689,696	4208.61	4.36	5.25		4.99								5.61									4.97		4.68	4.94	4.80	4.55
	4238.03	4.19	5.01	5.10	5.44										5.32				4.82			5.10			4.68	4.91	4.71
690	4228.71	2.73																							5.94	5.81	
692	4264.21	3.49	5.51		5.26	5.64													5.32			5.64			5.26	5.01	
693	4227.43	5.57	4.22		4.34	4.34				4.61			4.43		4.45	4.93	4.29		4.25			4.32	4.16	4.08	3.94	4.18	4.13
	4247.43	5.11	4.59	4.46	4.79	4.65									4.76	5.10	4.42		4.54			4.47	4.50	4.22	4.24	4.41	4.32
694	4087.10	3.98																			5.26	4.82					
	4136.51	3.70	4.83																5.59						5.30		5.05
694,695	4140.44	3.59				5.86															5.56		5.18		5.18		5.12
695	4157.79	4.97	4.42		4.66	4.98		5.46							5.09		4.99		4.70		4.73	4.90	4.44	4.31	4.43	4.44	4.45
698	4065.40	3.68																	5.04					4.68	4.93	4.81	4.97
	4072.52	4.10																	5.16			4.93	5.22		5.14	5.32	4.69
	4082.12	3.99								5.49			5.35		5.68									4.96	4.96	5.35	
	4084.50	4.74	4.40												5.01		5.14				4.72	4.64	4.45		4.28	4.33	4.47
	4133.87	4.52			5.32								5.30						5.02		4.85	4.97				4.74	4.38
726	4137.00	4.79	4.65	4.78	4.97			5.32							5.10	5.18	5.07		4.91		4.90	4.62	4.44	4.37	4.57	4.57	4.49
764	4240.37	3.69		4.76	5.29														5.63					4.98	5.26	5.14	
767	4059.73	4.06	5.43																			5.42		4.93	4.99	4.96	
797	4432.57	3.58	5.75		5.42																	6.23	5.58		5.59	5.68	
800	4219.36	5.50	4.51	4.61	4.72								4.93		4.91		4.86		4.57			4.65	4.36	4.33	4.54	4.46	4.55
816	6400.01	4.93	4.55																								
	6411.66	4.52	4.91																								
820	4596.06	4.46		5.07																		5.10	5.75		5.44	5.05	
	4643.47	4.16																				5.44			5.15	4.95	4.92
	4673.17	4.28																				5.41				5.14	4.78
822	4638.02	4.36																				5.40			5.21	4.96	
825	4495.99	3.48		5.84	6.06	6.28							5.46						5.36				5.44		5.47	5.84	
826	4611.28	5.02		5.12	4.89	5.21							5.44								5.21	4.93		4.46	4.76	4.93	4.58
828	4438.35	3.72																								5.69	
	4484.23	4.53	4.86	5.02	5.06	4.95							5.01									5.14		4.54	4.75	4.78	4.81

Mult. No.	λ	log gfλ	5110 .650	7080 .709	7085 .766	7091 .825		5616 .981		5647 .006		7102 .030		6207 .041		5617 .044		6211 .094		5618 .099		5651 .123	5556 .198	5058 .358	7010 .401	7013 .458	7017 .516
						l*	s*	l*	s*	l*	s*	l*	s*	l*	s*	l*	s*	l*	s*	l*	s*						
Fe I																											
43	4005.25	4.18	4.10					4.44	4.55			4.85	4.27	4.79	4.34		4.28		4.14		4.33	4.09	4.02	3.85	3.86	3.76	3.94
	4045.81	4.87	3.92					4.25	4.58	4.20	4.38	4.33	4.03	4.88	4.11	4.26	4.36	4.90	4.06	4.28	4.21	3.98	3.88	3.74	3.70	3.64	3.80
	4063.60	4.64	3.95					4.31		4.22	4.47	4.81	4.20		4.25	4.32	4.54		4.02	4.73	4.34	4.12	4.01	3.92	3.79	3.75	3.83
	4071.74	4.68	4.00					4.31	4.63	4.19	4.48	4.99	4.30	4.97	4.36	4.28	4.63		4.15	4.60	4.37	4.18	4.10	4.01	3.92	3.90	3.87
	4132.06	4.24	4.12	3.98	4.16	4.20				4.40	4.71		4.53	4.93	4.51	4.47	4.59		4.18		4.32	4.24	4.14	4.01	4.05	4.06	3.98
	4143.87	4.21	4.19	3.99	4.18	4.22	4.68	4.59				4.99	4.59			4.50	4.41		4.18	5.23	4.26	4.24	4.08		4.16	4.00	3.92
45	3815.84	4.80								4.04	4.32			4.48	4.07			4.76	4.24			4.08		3.93			
	3827.82	4.58								4.19	4.39				4.15	4.22	4.23		4.22			4.03		3.87			
	3841.05	4.57								4.28					4.33				4.29	4.50							
	3902.95	4.32							4.65	4.08	4.29				4.30	4.28	4.39		4.05		4.22	4.13				3.89	
62	6430.85	2.65	4.54																								
68	4430.62	2.91											5.00									4.91	4.50		4.59	4.73	
	4442.34	3.96	4.29	4.72	4.62	5.12		5.47					4.69		4.68							4.72			4.54	4.43	4.51
	4447.72	3.95	4.37	4.56	4.64	4.72													4.93			4.74	4.45	4.30	4.32	4.46	4.47
	4494.57	4.13	4.58	4.63	4.53	5.03							4.89				4.97		4.82			4.46	4.32	4.36	4.33	4.35	4.43
	4528.62	4.59	4.12	4.32	4.26	4.57							4.49		4.63				4.30		4.54	4.21	4.15	4.23	4.21	4.23	4.16
71	4282.41	4.32	4.28		4.41	4.35	4.79	4.78	5.20				4.62		4.96				4.35		4.56	4.35		4.27	4.28	4.31	4.26
	4352.74	3.60	4.52	4.46	4.65	4.91													4.83			4.47		4.46	4.30	4.39	4.35
111	6421.35	2.39	4.49																								
116	4439.88	1.96	5.89	5.34		5.80							5.89									6.36			5.89	5.59	5.16
117,853	4047.31	1.76																									5.24
152	4187.04	4.67	4.29	4.39	4.44	4.46							4.46				4.51		4.35		4.54	4.35		4.17	4.42	4.25	4.21
	4187.80	5.25	4.32	4.33	4.38	4.33		4.72					4.44		4.53	4.93	4.70		4.29		4.48	4.35	4.20		4.20	4.16	4.26
	4191.44	4.60	4.44	4.29	4.50	4.73							4.61		4.54				4.37			4.36			4.26	4.39	4.37
	4210.35	4.32	4.42	4.48	4.66	4.80		5.25					4.79		4.81	5.33	4.61		4.51			4.64	4.31	4.33	4.34	4.38	4.40
	4222.22	4.25	4.29	4.60	4.69								4.91			5.21	4.87		4.57			4.68	4.36	4.33	4.36	4.45	4.42
	4233.61	4.56			4.49							5.56	4.37						4.55			4.43	4.25		4.24	4.28	
	4235.94	4.87	4.30	4.19	4.51	4.60		4.95	4.85								4.48		4.38		4.50	4.30	4.22	4.26	4.23	4.26	4.13
	4250.12	4.66	4.41	4.23	4.46	4.53	4.88		4.76				4.69		4.67		4.46		4.37			4.35	4.22	4.24	4.13	4.29	4.36
	4260.48	5.07	4.24	4.20	4.30	4.21	4.55	4.76	4.73			5.32	4.41			4.98	4.58		4.29	4.99	4.12	4.28	4.15	4.18	3.98	4.10	3.96
	4271.16	4.71	4.31		4.51	4.54		4.81	4.99			4.70	4.43		4.69		4.67		4.31		4.30	4.41	4.26	4.26	4.16	4.25	4.19
206	6475.02	2.06	5.47																								
218	4049.34	2.82	4.94					5.80												6.18			4.83	5.16	4.87	4.65	4.81
268	6546.24	2.36	5.17																								
342	6518.38	2.40	5.05																								
350	4476.02	4.60	4.31	4.54	5.06								4.64		4.83		5.01		4.68			4.69	4.41	4.35	4.44	4.46	4.47
352	4245.26	4.24	4.71	4.72	5.12	5.26			5.39				5.18		5.36	5.33	5.10		4.87		4.60	4.66	4.44	4.45	4.57	4.46	4.45
354	4107.50	4.25	4.55	4.58	5.18	4.79		5.07	5.24	5.12					4.68	4.93	4.98		4.51	5.42	4.71	4.54	4.34		4.27	4.42	4.30
	4156.80	4.37	4.36	4.47	4.38	4.66							4.84		4.91				4.63	5.11	4.67	4.41			4.31	4.31	4.27
	4175.64	4.31	4.53	4.62	5.00	4.98							4.84		4.91				4.59		4.74	4.57	4.33	4.34	4.35	4.48	4.46
355	4154.50	4.35		4.55	4.77	4.58							4.78									4.37				4.35	
	4184.89	4.26											4.94						4.62		4.65	4.57	4.46	4.40		4.58	4.43
	4203.99	4.71	4.52	4.80	4.74	5.36							4.80		4.95		4.99		4.70		4.49	4.58	4.29	4.19	4.45	4.34	4.36
	4213.65	3.80	4.85	5.15	5.33	5.29										5.52	4.81		5.02			4.80	4.69	4.64	4.82	4.94	4.61
357	4091.56	2.83			5.08																	5.39				4.88	5.02
	4114.45	3.72	4.77	4.85	5.50	5.21			5.30	5.42					4.90		4.99			5.34	4.80	4.99	4.58	4.46	4.63	4.60	4.45
	4132.90	4.10	4.55	4.58	5.05								4.81		5.08				4.65			4.64	4.32	4.32	4.51	4.35	4.44
359	4044.61	4.42						5.49	5.17	5.26			4.73		5.00	5.11	4.86		4.95	5.17	5.19	4.80	4.31	4.40	4.57	4.45	
	4062.45	4.13	4.39					4.73					4.85		4.89		4.81		4.72	5.37	5.07	4.68	4.62		4.44	4.54	4.31
	4079.85	3.70																				4.81					
409	4647.44	3.92																				4.97	4.60		4.93	4.67	4.57
	4661.97	2.57																				5.82				5.45	5.14
	4691.41	3.72																				4.77				4.68	
	4710.29	3.77																									4.80
415	4365.90	3.49				5.75																			5.55	5.63	

VIII. Appendix

Mult. No.	λ	log gfλ	5110.650	7080.709	7085.766	7091.825 l*	7091.825 s*	5616.981 l*	5616.981 s*	5647.006 l*	5647.006 s*	7102.030 l*	7102.030 s*	6207.040 l*	6207.040 s*	5617.044 l*	5617.044 s*	6211.094 l*	6211.094 s*	5618.099 l*	5618.099 s*	5651.123	5556.198	5058.358	7010.401	7013.458	7017.516
Fe I																											
828,848	4479.61	4.31											5.22									5.46				5.34	4.85
830	4388.41	4.63											5.21									5.07				5.04	4.68
	4433.22	4.68			4.97	5.97		5.37					5.04						5.40			5.42			4.91	5.30	4.61
	4485.68	4.16			5.24																		5.16			5.59	5.12
906	4246.09	4.67	5.82	5.10	5.82														5.54			5.62			5.01	4.96	4.93
973	4494.05	3.70																									4.97
976	4276.68	3.88	5.39			5.26													5.57			5.78		5.10	5.44	5.16	5.26
	4300.83	3.89																									4.59
993	4264.74	3.58																								6.04	
993,994	4265.26	3.93		5.58		5.80			5.78														5.74		5.92		
1042	4735.85	4.24																									5.00
1068,821	4745.81	4.44																									4.85
Fe II																											
27	4128.73	'3.84	4.90	4.47	4.99	5.18							4.84		4.87		5.01		4.96		4.82	4.74	4.44		4.53	4.54	
	4233.17	5.55			4.24	4.12		4.25	4.68			4.45	4.30		4.30		4.69		4.16		4.22	4.35	4.13		4.08	4.28	
	4303.17	5.02	4.38	4.50	4.43	4.43		4.55				4.74	4.37						4.42			4.50	4.22	4.15	4.26	4.24	4.23
	4385.38	5.26	5.10	4.38	4.37	4.58			4.82			4.65	4.52		4.47				4.29	5.48	4.67	4.47	4.35	4.14	4.30	4.21	4.31
	4416.82	4.94		4.60	4.41	4.47		4.54	5.13				4.55		4.59				4.39		4.44			4.34	4.40	4.32	4.25
28	4178.85	5.03				4.56								4.85	4.34		4.89		4.27		4.31	4.29	4.23	4.15		4.22	4.19
	4296.57	5.13	4.22		4.87	4.60		4.78	5.14			5.18	4.67			4.98	4.99		4.45	5.60	4.43	4.34	4.32	4.23	4.43	4.35	4.33
	4369.40	3.94	4.88	4.72	4.90	4.85							5.05		5.07				4.82					4.49	4.64	4.63	4.50
37	4472.92	4.60	4.54		5.00	5.34							4.74	5.62	4.82				4.92		4.72	4.68		4.29	4.48	4.58	4.45
	4489.18	4.81	4.48	4.61	4.65	4.65		4.68	5.12				4.42		4.54	4.90	4.75		4.78		4.59	4.60		4.32	4.56	4.42	4.33
	4491.40	4.84	4.68	4.66		5.03		4.85	5.45				4.61		4.48	4.92	4.73		4.49		4.55	4.39	4.43	4.29	4.55	4.33	4.45
	4515.34	5.19	4.51	4.50	4.68	4.46	4.61	4.66	5.20			4.80	4.51	4.73	4.44				4.31		4.53	4.54	4.31	4.28	4.33	4.27	4.26
	4520.22	5.11	4.31	4.53	4.66	4.52		4.64	5.11			4.73	4.55	4.81	4.41				4.36		4.71	4.43	4.36	4.30	4.28	4.30	4.31
	4582.83	4.37	4.72	5.15	5.25								4.70		4.91				4.93			4.68	4.46	4.38	4.47	4.48	4.55
	4666.75	4.29																				5.03			4.59	4.53	
38	4508.28	5.19	4.46	4.35	4.62	4.81		4.54	4.91			4.74	4.52	4.52	4.52	5.12	5.11		4.53		4.70	4.42	4.31	4.23	4.51	4.21	4.31
	4522.63	5.81	4.15	4.21	4.26	4.27		4.65	4.89			4.59	4.38	4.73	4.43				4.29	4.84	4.46	4.26	4.13	4.10	4.17	4.17	4.15
	4541.52	4.65	4.66	4.69	5.09	4.67									4.49				4.67	5.36	4.59	4.63	4.55	4.28	4.39	4.37	4.43
	4576.33	4.53	4.49		5.27	4.81							4.74		4.69				4.74		4.59	4.73	4.45	4.26	4.48	4.49	4.47
	4583.83	5.66	4.34	4.21	4.10	4.20		4.61	4.99			4.34	4.32	4.76	4.48				4.23	4.46	4.30	4.20		4.07	4.11	4.24	4.12
	4620.51	4.17	4.84	4.82									4.99									4.93	4.51	4.40	4.83	4.64	4.66
43	4731.44	4.39																									4.39
Mg II																											
4	4481.2		4.30			4.28		4.41					4.10			5.04	4.37			4.50	4.38			4.11		4.28	
9	4427.99							5.72													5.36			5.02			
Ba II																											
1	4554.03		4.11	3.99	4.06	4.04	4.96	4.33	4.68			5.02	4.60		4.86				4.34	4.65	4.37	4.38	4.17	4.02	4.01	4.07	4.00
Sr II																											
1	4077.71		3.99					4.25	4.48	4.08	4.39	4.16	4.24	4.58	4.24	4.12	4.27	4.39	4.03	4.28		4.07	3.97	3.71	3.75	3.73	3.76
	4215.52		4.01	3.96	3.96	3.95	4.63			4.16	4.54		4.40		4.46	4.12	4.41		4.31			4.22	4.11	3.99	3.84	3.89	3.90
Sc II																											
7	4246.83		4.32	4.08	4.19	4.23	5.04	4.32	5.09	4.29			4.77	4.72			4.57		4.54			4.63	4.33	4.21	4.26	4.32	4.28
Ca I																											
2	4226.73		3.83	3.85	4.04	3.88				4.11	4.38		4.19		4.28				4.06			4.07	3.92	3.88	3.91	3.83	3.74